

Effective Gauge Theories, The Renormalization Group, and High- T_c Superconductivity. *

A. Campbell-Smith and N.E. Mavromatos.

Theoretical Physics, (University of Oxford), 1 Keble Road, Oxford, OX1 3NP, U.K.

Abstract

These lectures serve as an introduction to the renormalization group approach to effective field theories, with emphasis on systems with a Fermi surface. For such systems, demanding appropriate scaling with respect to the renormalization group for the appropriate excitations leads directly to the important concept of quasiparticles and the connexion between large- N_f treatments and renormalization group running in theory space. In such treatments N_f denotes the number of effective fermionic degrees of freedom above the Fermi surface; this number is roughly proportional to the size of the Fermi surface. As an application of these ideas, non-trivial infra red structure in three dimensional U(1) gauge theory is discussed, along with applications to the normal phase physics of high- T_c superconductors, in an attempt to explain the experimentally observed deviations from Fermi liquid behaviour. Specifically, the direct current resistivity of the theory is computed at finite temperatures, T , and is found to acquire $\mathcal{O}(1/N_f)$ corrections to the linear T behaviour. Such scaling corrections are consistent with recent experimental observations in high T_c superconducting cuprates.

*Based on lectures given by N.E.M. at the XXXVIII Cracow School of Theoretical Physics, *New Quantum Phases, Elementary Excitations and Renormalization in High Energy and Condensed Matter Physics*; Zakopane, Poland; June 1-10, 1998.

Contents

1	Introduction.	3
2	Lecture I (i): Effective Field Theory.	4
2.1	Generic analysis of Wilsonian approach.	4
2.2	Renormalization group flow equations: β -functions.	5
2.2.1	Example: a single marginal coupling.	6
2.2.2	Super-renormalizable (relevant) couplings: naturalness.	6
2.3	Concluding remarks.	7
3	Lecture I (ii): The Renormalization Group, Fermions And The Fermi Surface.	7
3.1	Generic analysis.	7
3.2	Quasiparticles.	8
3.3	Exercises.	10
3.3.1	BCS Pairing interactions as deviations from Fermi liquid theory.	10
3.3.2	BCS vs Phonon-electron pairing.	11
3.4	Landau's Fermi liquid from a renormalization group viewpoint.	11
3.5	Concluding remarks.	12
4	Lecture II (i): Non-Trivial Infra Red Structure in QED₃.	12
4.1	Zero temperature analysis of QED ₃	13
4.2	Studies in the $p \gg \alpha$ region.	16
4.3	Studies in the $p \lesssim \alpha$ regions: the wavefunction renormalization.	17
4.4	The vertex <i>ansatz</i> and the wavefunction renormalization.	17
4.4.1	Simplified treatments.	18
4.4.2	More refined treatments.	18
4.5	The infra red cut-off.	19
4.5.1	Graphical results.	20
4.5.2	Remark: generic Wilsonian renormalization approach to U(1) gauge theory.	22
4.6	Composite operator effective potential approach.	22
4.7	The physical consequences of "slow running."	23
4.8	Exercises.	24
4.8.1	The Dyson-Schwinger equations.	24
4.8.2	Dyson-Schwinger vs composite operator effective potential.	24
4.9	Concluding remarks.	24
5	Lecture II (ii): Results Beyond Leading Order in $1/N_f$.	24
5.1	Non-local gauges.	25
5.2	Infra red critical exponents beyond $1/N_f$ from the non-local gauge.	25
5.3	Improved computation of behaviour beyond $1/N_f$	27
5.4	An alternative description of running flavour number.	28
5.5	Concluding remarks.	28
6	Lecture II (iii): Predictions of Gauge Interactions for Finite Temperature Models.	29
6.1	The resistivity in gauge field theory models.	29
6.2	The real time formalism and Landau damping.	30
6.3	Spin-charge separation and resistivity.	31
6.3.1	Resistivity and Ohm's law.	31
6.3.2	The spin-charge separation formalism.	31
6.3.3	Speed of light in non-trivial vacua.	32
6.3.4	Logarithmic corrections to the resistivity.	33
6.4	Comparison with other approaches.	34
7	Conclusions.	35

1 Introduction.

The concept of effective field theory [1–4] is an old one, and has wide applications in physics, ranging from condensed matter to high energy physics and cosmology. The effective field theory method isolates properly those degrees of freedom in a dynamical system which are driving the dynamics in a certain range of energy–momentum.

Formally, an effective field theory is represented by a functional integral in which we perform an appropriate splitting of the field–theoretic degrees of freedom $\{\phi(x)\}$:

$$\{\phi(x)\} = \{\phi_H(x)\} + \{\phi_L(x)\}. \quad (1.1)$$

The fields ϕ_H (ϕ_L) have Fourier components corresponding to momenta $k > \Lambda$ ($k < \Lambda$) where Λ is a characteristic energy scale in the problem which *defines* the low energy effective dynamics. Now the effective field theory below the scale Λ is obtained formally by integrating out the high–frequency modes ϕ_H in the functional integral. What remains after the integrations defines the *effective Lagrangian density* $\mathcal{L}_{\text{eff}}(\phi_L, \dot{\phi}_L)$ which is an infinite series in a derivative expansion and describes the low energy dynamics. The issue of whether the splitting (1.1) can always lead to a meaningful effective theory is a very complicated one, and in general depends on the details of the dynamics and the cut–off scale Λ . In most cases of interest, however, the concept of an effective theory is useful in describing the basic features of the underlying dynamics (below the scale Λ) in a simple way.

One of the most important tools in the study of effective field theories is the renormalization group [1,5–7]. This technique allows one to group effective field theories with apparently very different interactions into categories which emphasise their common features, e.g. similar scaling exponents of certain correlation functions (which can be measured experimentally). Such groups of effective theories are termed “universality classes” and prove essential in understanding the similar properties of ostensibly different physical systems: all systems in the same universality class flow to the same renormalization group fixed point [1].

The aim of this set of lectures is to introduce the concept of an effective field theory and the associated renormalization group techniques, first in a generic way, and later on through some specific and physically interesting examples; these will include the BCS superconductivity phenomenon (as a guided exercise for the reader) and a possible explanation of the abnormal properties of high–temperature superconductors in their normal phase.

The structure of the lectures is as follows: in the first half of the lectures (sections 2–3) the basic features of the renormalization group approach to effective field theories is discussed briefly. Particular attention is paid to discussing scaling properties of systems with a Fermi surface, relevant for condensed matter applications. The important concept of quasiparticles is introduced in section 3. There are excitations of the Fermi surface which are appropriately dressed so as to have the correct scaling under the renormalization group.

An interesting application concerning the representation of the Landau Fermi liquid theory as a theory with a trivial infra red fixed point concludes the first half of the lectures. In this model the quasiparticle degrees of freedom below a scale Λ appear as fermions with a Λ –dependent “flavour number” $N_f(\Lambda)$, which runs to infinity as $\Lambda/P_F \rightarrow 0$ (P_F being the typical size of the Fermi surface).

In the second half of the lectures (section 4 ff.) a second application of the renormalization group and effective theories is considered: that of trying to understand the abnormal behaviour of high temperature superconductors in their normal (chirally symmetric) phase in terms of deviations from the Fermi liquid trivial infra red fixed point. In the context of the gauge theory approach to the physics of doped antiferromagnets, believed to simulate the physics of high temperature superconductivity, it is demonstrated using methods of effective field theory that three dimensional U(1) gauge theory (QED₃) is characterized by a non–trivial infra red fixed point. The fermion–gauge field interaction vertex becomes marginally relevant and drives the theory to non–Fermi liquid behaviour in the infra red. The fixed point structure is non–perturbative and is discovered using a renormalization group improved Dyson–Schwinger analysis [8].

The interesting feature of the QED₃ Dyson–Schwinger resummed problem is that the “running” coupling coincides with the inverse of a fermion flavour number, thereby providing an interesting application of the above–mentioned effective running of flavour number in the context of condensed matter physics. Some physical consequences of this phenomenon, concerning the scaling of the electrical resistivity in QED₃ at finite temperature are discussed with the aim of comparing the results with the phenomenology of the normal phase of high temperature superconductors (section 6).

Finally, we present conclusions and outlook in section 7.

2 Lecture I (i): Effective Field Theory.

2.1 Generic analysis of Wilsonian approach.

Consider a field theory in which an energy scale E_0 is introduced. This energy scale need not be associated with the normal divergence-cancelling cut-offs in field theory. Effective field theory is a method for analysing the physics at lower energy scales $E \ll E_0$. To construct the effective field theory, split the fields into high and low frequency components ϕ_H and ϕ_L with frequencies above and below the scale $\Lambda \sim E_0/\hbar$ respectively (from here on $\hbar \equiv 1$):

$$\{\phi(\omega)\} = \{\phi_H(\omega)\} + \{\phi_L(\omega)\} \quad (2.1)$$

where

$$\begin{aligned} \{\phi_H(\omega)\} &= \{\phi(\omega) : \omega > \Lambda\}, \\ \{\phi_L(\omega)\} &= \{\phi(\omega) : \omega < \Lambda\}; \end{aligned} \quad (2.2)$$

in general the split can be performed smoothly or sharply: the specifics of the split will not matter here.

Now the high-frequency components ϕ_H are integrated out in the functional integral

$$\int D\phi_L \int D\phi_H e^{iS(\phi_H, \phi_L)} = \int D\phi_L e^{iS_\Lambda(\phi_L)}, \quad (2.3)$$

and the *Wilsonian effective action* $S_\Lambda(\phi_L)$ is given by

$$e^{iS_\Lambda(\phi_L)} = \int D\phi_H e^{iS(\phi_L, \phi_H)}. \quad (2.4)$$

The effective action S_Λ can be expanded in a complete set of local operators:

$$S_\Lambda = S_0(\Lambda, g^*) + \sum_i \int d^D x g^i \Theta_i, \quad (2.5)$$

where the sum runs over all local operators Θ_i allowed by the symmetries of the model and the $\{g^i\}$ are the associated couplings, which may be thought of as coordinates in coupling space. The set of couplings $\{g^*\}$ denote the (trivial) fixed point of the theory (see section 2.2), which for convenience can be chosen to be $g^* = 0$ (the origin of coupling space) so that the expansion point S_0 is the free action. Some elementary dimensional analysis from the free action yields the *scaling dimension* of the operators and couplings:

$$\begin{aligned} \Theta_i &\rightarrow E^{h_i}, \\ g^i &\rightarrow E^{D-h_i}. \end{aligned} \quad (2.6)$$

These scalings can be used to derive a dimensional estimate of the magnitude of an operator in S_Λ ,

$$\int d^D x \Theta_i \sim E^{h_i - D}.$$

Introducing the dimensionless couplings

$$\lambda^i = g^i \Lambda^{h_i - D}, \quad (2.7)$$

it can be seen that the i^{th} term in the action is of order

$$\lambda^i \left(\frac{E}{\Lambda}\right)^{h_i - D}. \quad (2.8)$$

Using this dimensional estimate, the operators in the expansion (2.5) can be classified according as the value of $h_i - D$ is positive, negative or vanishing; see table 2.1. If $h_i - D < 0$ the operator becomes more

$h_i - D$	Size as $E \rightarrow 0$	Type of Operator	Type of Theory
< 0	Grows	Relevant	Super-renormalizable
0	Constant (scale invariant)	Marginal	Strictly renormalizable
> 0	Decays	Irrelevant	Non-renormalizable

Table 1: Classification of operators in an effective field theory.

important at lower energies, and is called *relevant*. An operator with vanishing $h_i - D$ is equally important at all energies and is called *marginal*. Operators with $h_i - D > 0$ are *irrelevant*, for they become less and less important at low energies.

The lesson to be learned from the power counting above is that the low energy physics is only sensitive to the high energy theory through the marginal and relevant couplings. In most cases there is a finite number of relevant and marginal couplings, so in principle the low energy physics depends on only a finite number of parameters. There are subtleties, however, due to possible infra red structure, i.e. divergences in the low energy theory. The simple power counting above is done from the free action, and so the interactions present in the full effective action (2.4) can affect the behaviour: operators can change between being marginal, relevant and irrelevant as a result of the interactions.

2.2 Renormalization group flow equations: β -functions.

The scaling derived from simple power counting is modified by interactions in the effective theory; these effects are encoded in the β -function. The β -functions for the renormalized couplings $g^i(E)$ are defined as follows:

$$\beta^i \equiv E \frac{\partial}{\partial E} g^i(E) = y^i g^i(E) + C_{jk}^i g^j g^k + \dots, \quad (2.9)$$

where y^i are the anomalous dimensions (due to quantum corrections) and the C_{jk}^i are the coefficients of the operator product expansion pertaining to the three-point functions of the theory:

$$\langle \Theta_i(x_1) \Theta_j(x_2) \Theta_k(x_3) \rangle_0 = C_{ijk} |x_{12}|^{\delta_{ij}-D} |x_{13}|^{\delta_{ik}-D} |x_{23}|^{\delta_{jk}-D}, \quad (2.10)$$

where $\delta_{ij} = y_i + y_j - y_k$, etc., $|x_{ij}| = |x_i - x_j|$ and where $\langle \dots \rangle_0$ indicates correlators taken with respect to $S_0(\Lambda, g^*)$ (see equation (2.5)).

In coupling space indices are raised and lowered by the so-called Zamolodchikov [9] metric:

$$G_{ij} = |x|^{2D-y_i-y_j} \langle \Theta_i(x) \Theta_j(0) \rangle_{S_\Lambda} \quad (2.11)$$

where now the symbol $\langle \dots \rangle_{S_\Lambda}$ indicates correlators taken with respect to the full (interacting) action, equation (2.4). The covariant coefficients C_{ijk} appearing in the three-point functions are totally symmetric in their indices.

Close to the fixed point (at least to order g^2), the β -functions defined above are related [10] to a gradient flow in coupling space

$$\partial_i \Phi(g, g^*, \Lambda) = G_{ij}(g^*, \Lambda) \beta^j(g, g^*, \Lambda). \quad (2.12)$$

The renormalization group invariant flow function Φ in two dimensional systems has been related to the components of the stress tensor of the theory [9]. In higher dimensions Φ is still not known in closed form, although attempts have been made to relate it to stress tensor components by appropriate extension of the two dimensional case [11]. Notice that the total symmetry of C_{ijk} is crucial [10] for the gradient flow (2.12).

In the case of two dimensional unitary theories the metric G_{ij} is manifestly positive definite [9] and hence relations like equation (2.12) imply, in view of the renormalization group invariance of Φ , that the flow function decreases along the renormalization group trajectories in coupling space:

$$\partial_t \Phi = -\beta^i \partial_i \Phi = -\beta^i G_{ij} \beta^j < 0, \quad (2.13)$$

where $t = \ln(E/\Lambda)$ is a renormalization group scale. According to reference [9] the value of the flow function at a fixed point coincides with the central charge of the corresponding two dimensional conformal field theory. Hence the relation (2.13) implies that under relevant perturbations a unitary theory flows along a direction of decreasing central charge. This poses interesting restrictions on the flow of two dimensional theories which might have interesting physical applications [12]. In higher dimensions the proof of such an irreversibility is not yet complete but recently there have been interesting attempts [11]. Such a theorem on the irreversibility of the renormalization group flow in D dimensions is expected to hold on general grounds for effective field theories are plagued by loss of information from the modes above the scale Λ which are integrated out. Such modes contribute a non-zero entropy change which in the case of two dimensional physics has been shown to correspond to the flow function Φ .

2.2.1 Example: a single marginal coupling.

A single marginal coupling will typically have a β -function as follows:

$$\beta^g = bg^2 + \mathcal{O}(g^3), \quad (2.14)$$

which can readily be integrated to give the solution

$$g(E) = \frac{g(\Lambda)}{1 + bg(\Lambda) \ln\left(\frac{\Lambda}{E}\right)}. \quad (2.15)$$

For $b > 0$ the coupling decreases at low energies and is marginally irrelevant. If $b < 0$ the coupling grows and is marginally relevant. A strictly marginal coupling is only obtained if the β -function vanishes to all orders in g . So it is seen that the physics of a system with a marginal coupling depends on the details of the problem, here encoded in b . A marginally relevant coupling can lead to interesting effects; for example, in QCD a marginally relevant coupling leads to confinement and chiral symmetry breaking; similarly in condensed matter models of the resistivity in the presence of magnetic impurities, the Kondo effect [13] leads to an increase in the resistivity in the deep infra red (the very low temperature region).

For a single coupling the gradient flow relation (2.12) is trivial to prove. It is not at all trivial to prove the relation for models with more than one coupling, for the existence of a gradient flow requires the curl-free condition on the quantity $G_{ij}\beta^j$. This has been shown in D dimensions at least in the neighbourhood of a fixed point (to order g^2) in reference [10].

2.2.2 Super-renormalizable (relevant) couplings: naturalness.

In effective field theories, non-renormalizable terms do not cause problems, for there is an ultra violet cut-off which automatically acts as a regulator for the associated divergences. Indeed, non-renormalizable terms *have* to appear at some scale in the effective theory: in fact the information about where the cut-off must lie is encoded in these terms. For effective field theories there is a new problem, not found in conventional field theories: super-renormalizable terms, which grow below the cut-off. This means that, without unnatural fine-tuning of the original parameters, all masses in the effective field theory must be of order of the cut-off; this is a contradiction, however, for such fields cannot appear in the effective theory at all. So effective theories must be *natural*, meaning that there must exist symmetries which force the masses to vanish. A pertinent example of this is the $U_S(1)$ effective gauge field theory of doped antiferromagnets at the d -wave gap (see section 6.3.2): the charged excitations are described by Dirac fermions whose masses are forced to vanish by chiral symmetry; there are also gauge fields forced massless by gauge invariance. To include scalars in a model their masses must be forbidden by Goldstone's theorem or supersymmetry.

There is also a problem with super-renormalizable interactions: at scales below the cut-off, the (dimensionless) coupling will grow to larger than unity, and hence the low energy theory may be described by new

degrees of freedom: bound states, condensates, etc. An exception to this is when the infra red behaviour is governed by a (non-trivial) fixed point, in which case the theory may still be described by the original degrees of freedom. An example is QED₃ (see section 4), which is super-renormalizable, but renormalization group improved Dyson–Schwinger analysis reveals a non-trivial infra red fixed point [8]. As will be discussed later in lecture II (section 4 ff.) this is relevant for the normal phase of high-T_c superconductors.

2.3 Concluding remarks.

- Effective field theory is a tool for understanding the physics of renormalization.
- Interactions in an effective field theory can be classified as *relevant*, *marginal*, or *irrelevant* according to their scaling properties.
- The infra red physics is only sensitive to the high energy theory through the marginal and relevant couplings.
- When a marginal coupling grows large, interesting physics can result.
- Interesting physics can also arise when a super-renormalizable coupling is driven to a non-trivial infra red fixed point.
- Naturalness: effective theories must be *natural*, in that there must exist symmetries which force parameters which would naturally appear at $\mathcal{O}(\Lambda)$ to vanish.

3 Lecture I (ii): The Renormalization Group, Fermions And The Fermi Surface.

3.1 Generic analysis.

Now the renormalization group approach is applied to the theory of the Fermi surface in condensed matter systems. This will demonstrate the need for the concept of quasiparticles and the provide motivation for large- N_f treatments (N_f = flavour number) [4].

Slice momentum space into the following sets: $I_1, I_0, I_{-1}, I_{-2}, \dots$

$$\begin{aligned}
 I_1 &= \left\{ (k_0, \vec{k}) : k_0^2 + \left[\frac{(\vec{k}^2 - P_F^2)}{2m} \right]^2 \geq P_0^2 \right\} \\
 I_n &= \left\{ (k_0, \vec{k}) : (2^{n-1}P_0)^2 \leq k_0^2 + \left[\frac{(\vec{k}^2 - P_F^2)}{2m} \right]^2 \leq (2^n P_0)^2 \right\} \quad n \leq 0. \quad (3.1)
 \end{aligned}$$

The scale P_0 is arbitrary, e.g. the inverse of the range of the potential. The Fermi sphere is defined by: $(k_0, |\vec{k}| = P_F)$, and $(2^n P_0)$ is a measure of the distance of the n^{th} layer from the Fermi surface.

The fermion propagator is given by [14]

$$G(t, \vec{x}) = \sum_{n=-\infty}^{n=1} G^{(n)}(t, \vec{x}) \equiv \sum_{n=-\infty}^{n=1} \int_{I_n} \frac{dk_0 d^d k}{(2\pi)^{d+1}} \frac{e^{-i(k_0 t + \vec{k} \cdot \vec{x})}}{-ik_0 + (\vec{k}^2 - P_F^2)/2m}. \quad (3.2)$$

The n^{th} summand $G^{(n)}$ is the contribution to the propagator coming from the layers at a distance $\mathcal{O}(2^n P_0)$ from the Fermi surface. This decomposition of the propagator generates a representation for the fermionic fields:

$$\Psi_{\vec{x}}^{\pm} = \sum_{n=-\infty}^{n=1} \Psi_{\vec{x}}^{(n)\pm}, \quad (3.3)$$

where the plus and minus signs are respectively for “particles” and “holes.”

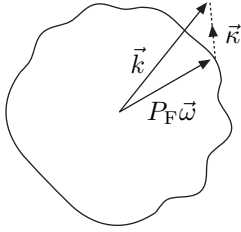


Figure 1: The Fermi Surface of effective radius $\mathcal{O}(P_F)$ (assuming a near-spherical shape), showing the quasiparticle momentum as measured from the surface.

There is a difficulty with the application of renormalization group techniques to this non-relativistic field theory. This is illustrated by an example in three dimensions [4]: for large n and large $|\vec{x}| + |t|$, it can be shown that

$$G^{(n)}(t, \vec{x}) \sim 2^{2n} m P_F P_0 \left[t \frac{\sin(P_F |\vec{x}|)}{P_F |\vec{x}|} + \frac{m \cos(P_F |\vec{x}|)}{P_F} \right] \mathcal{G}(2^n t P_0, 2^n \vec{x} P_0). \quad (3.4)$$

While the function \mathcal{G} scales normally, i.e. depends on (t, \vec{x}) only as $(2^n P_0 t, 2^n P_0 \vec{x})$, there is a problematic oscillation on a scale P_F^{-1} and a scaleless singularity $|\vec{x}|^{-1}$ so overall the propagator does not scale properly. This is unlike the situation in relativistic field theories as discussed in the section 2 where P_F is vanishing; so how can fields be assigned scaling dimensions and how can couplings be identified as marginal, relevant or irrelevant? The resolution is in the concept of quasiparticles [4], which are the subject of the next subsection.

3.2 Quasiparticles.

Consider the following expansion of the particle/hole fields:

$$\Psi_{\vec{x}}^{\pm} = \int_{|\vec{\omega}|=1} d\vec{\omega} e^{\pm i P_F \vec{\omega} \cdot \vec{x}} \Psi_{\vec{x}, \vec{\omega}}^{\pm}. \quad (3.5)$$

The integration is over the unit sphere, and so $P_F \vec{\omega}$ is a momentum on the Fermi sphere.

Inserting the Fourier transform of $\Psi_{\vec{x}, \vec{\omega}}^{\pm}$,

$$\Psi_{\vec{x}}^{\pm} = \int d\vec{k} \int_{|\vec{\omega}|=1} d\vec{\omega} e^{\pm i (P_F \vec{\omega} - \vec{k}) \cdot \vec{x}} \tilde{\Psi}_{\vec{x}, \vec{\omega}}^{\pm} \quad (3.6)$$

So here the quantity $-\vec{\kappa} = P_F \vec{\omega} - \vec{k}$ plays the rôle of a momentum, as measured from the surface of the Fermi surface (see figure 1). The integration over the orientation $\vec{\omega}$ has to be performed at the very end of the computations.

The advantage of using the quasiparticle degrees of freedom was indicated in the last section; it is because they have the correct scaling behaviour and so admit a conventional renormalization group treatment. The quasiparticle propagator reads:

$$G^{(n)}(\vec{x}, \vec{\omega}; \vec{x}', \vec{\omega}') = \delta(\vec{\omega} - \vec{\omega}') G^{(n)}(\vec{x} - \vec{x}'; \vec{\omega}). \quad (3.7)$$

Now for large n it is possible to show [4] that the quasiparticles scale in all dimensions (D) like $2^{n/2}$ and hence have mass dimension $\frac{1}{2}$:

$$G^{(n)}(\vec{x}, \vec{\omega}) \sim 2^n P_F^{D-1} P_0 (2^n P_0 t - 2i P_0 \vec{\omega} \cdot \vec{x}) G^{(n)}(2^n P_0 \vec{x}). \quad (3.8)$$

Quasiparticles appear as a consequence of non-trivial Fermi surfaces, about points at which the dispersion relation has been linearized. To illustrate, a model in $2 + 1$ dimensions is considered, which is relevant for there is the possibility of applications to the physics of high- T_c superconductors. First, slice the orientation

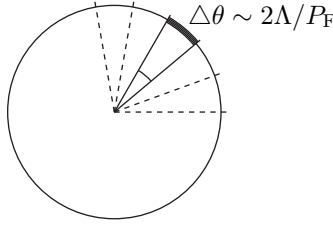


Figure 2: The orientation space is sliced into angular cells. Note that the width of the cells could in principle be some function of Λ/P_F .

space into angular cells (see figure 2). For spherical Fermi surfaces, the angular integration can be replaced by a sum:

$$\int_{|\vec{\omega}|=1} d\vec{\omega} \longrightarrow P_F \int_0^{2\pi} \frac{d\theta}{2\pi} \longrightarrow \sum_i, \quad (3.9)$$

where the sum is over the angular cells, each of which has width

$$\Delta\theta = \frac{2\Lambda}{P_F} \quad (3.10)$$

and where Λ is some ultra violet cut-off in the theory. There are

$$N = \frac{2\pi P_F}{2\Lambda} \quad (3.11)$$

cells labelled by i [3]. At each cell the momentum can be written as follows:

$$\vec{k}_i = P_F \vec{\omega}_i + \kappa_i^\parallel \vec{\omega}_i + \kappa_i^\perp \vec{t}_i \equiv P_F \vec{\omega}_i + \vec{\kappa}_i. \quad (3.12)$$

The κ_i^\parallel are the radial components of the momentum, κ_i^\perp are the angular displacements from the centre of the cell and the \vec{t}_i are tangent unit vectors on the Fermi surface which form a basis for the angular displacements κ_i^\perp . Therefore:

$$\int \frac{d^2 k}{(2\pi)^2} \equiv \int_{-\Lambda}^{\Lambda} \frac{dk}{2\pi} P_F \int_{-\Lambda/P_F}^{\Lambda/P_F} \frac{d\theta}{2\pi} = \int_{-\Lambda}^{\Lambda} \frac{d\kappa^\parallel}{2\pi} \int_{-\Lambda}^{\Lambda} \frac{d\kappa^\perp}{2\pi}. \quad (3.13)$$

Note that the size of each cell, equation (3.10), need not be a simple function of Λ/P_F . More generally each cell may be allowed to have a size $f(\Lambda/P_F)$ which can be determined from the renormalization group scaling; in what follows, and in section 4 for the case of three dimensional U(1) gauge theory, a connexion will be made between the function f and the flavour number.

In this 2 + 1 dimensional model the kinetic term for free fermions in the current formalism is as follows:

$$S_0 = \sum_{i=1}^N \int \frac{d^2 \kappa_i d\kappa_i^0}{(2\pi)^3} \bar{\Psi}_i(\vec{\kappa}_i, \kappa_i^0) [i\kappa_i^0 - v^* \kappa_i] \Psi_i(\vec{\kappa}_i, \kappa_i^0). \quad (3.14)$$

The model has the following interaction terms:

$$S_F = -\frac{1}{P_F} \sum_{i,j=1}^N \int d\mathcal{F} \bar{\Psi}_j(\vec{\kappa}_4, \kappa_4^0) \Psi_j(\vec{\kappa}_2, \kappa_2^0) F_{ij} \bar{\Psi}_i(\vec{\kappa}_3, \kappa_3^0) \Psi_i(\vec{\kappa}_1, \kappa_1^0), \quad (3.15)$$

where the measure $d\mathcal{F}$ is

$$d\mathcal{F} = \left(\prod_{\ell=1}^4 d^3 \kappa_\ell \right) \delta(\kappa_1^0 + \kappa_2^0 - \kappa_3^0 - \kappa_4^0) \delta^{(2)}(\vec{\kappa}_1 + \vec{\kappa}_2 - \vec{\kappa}_3 - \vec{\kappa}_4),$$

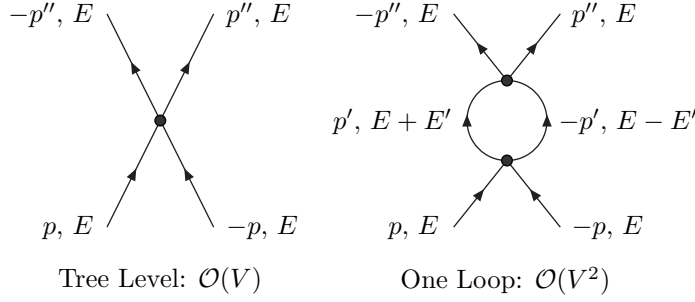


Figure 3: Four–electron interaction at tree level and one loop.

and the coupling is

$$F_{ij} = F \vec{\omega}_i \cdot \vec{\omega}_j.$$

Now, expressing all the momenta $\vec{\kappa}$ and frequencies κ_0 in terms of the cut–off Λ it can be seen that the only place where Λ appears is in front of the interaction term, in the combination Λ/P_F . This is to be compared with large– N_f models under the replacement:

$$f\left(\frac{\Lambda}{P_F}\right) \longleftrightarrow \frac{1}{N_f}. \quad (3.16)$$

Here N_f can be interpreted as the effective area of the Fermi surface [15]. For kinematical reasons the most important interactions are between $\bar{\Psi}\Psi$ *in the same cell* [2]. In order to allow for maximum momentum transfer within the framework of the effective theory (i.e. remaining close to the Fermi surface) interactions between excitations well separated on the generic Fermi surface (not exhibiting nesting) are suppressed. Nesting is of course the case of BCS instabilities, which is the subject of the exercise in section 3.3. The infra red limit of the 2 + 1 dimensional model considered ($\Lambda \ll P_F$) corresponds to the $N_f \rightarrow \infty$ limit in the large– N_f model. Thus the qualitative effect of the “quasiparticles” is to increase the effective number of flavours, where here the flavours are the internal degrees of freedom due to the Fermi surface. Note, however, that N_f depends on the cut–off and therefore there is a renormalization group running in “theory space” as discussed in sections 4 ff.

3.3 Exercises.

3.3.1 BCS Pairing interactions as deviations from Fermi liquid theory.

Consider a constant four–electron interaction in BCS theory (see figure 3):

$$V(k_1, k_2, k_3, k_4) = \text{const} = V. \quad (3.17)$$

Concentrate on the one loop term:

$$I = V^2 \int \frac{dE' d^2k' d\ell'}{(2\pi)^4} \frac{1}{[(1+i\epsilon)(E+E') - v_f(k')\ell']} \frac{1}{[(1+i\epsilon)(E-E') - v_f(k')\ell']}. \quad (3.18)$$

Here k is the momentum component parallel, and ℓ the component perpendicular to the Fermi surface.

Compute the leading logarithmic divergences of I , I_{ln} , and show that

$$I_{\text{ln}} \sim V^2 N \ln\left(\frac{E_0}{E}\right) + \mathcal{O}(V^3), \quad (3.19)$$

where

$$N \sim \int \frac{d^2k'}{(2\pi)^3} \frac{1}{v_f(k')} \sim \text{density of states at Fermi energies}. \quad (3.20)$$

Write down a renormalization group flow equation for

$$V(E) = V - I_{\ln}$$

and solve it to show that

$$V(E) \sim \frac{V}{1 + NV \ln(E_0/E)}. \quad (3.21)$$

Hence the BCS interactions are marginally relevant if attractive ($V < 0$) and grow stronger as $E \rightarrow 0$.

3.3.2 BCS vs Phonon–electron pairing.

Assume a screened Coulomb interaction $V_c = \text{const}$ for simplicity. Define its coupling $\mu = NV_c$ and write down a renormalization group flow equation for it. Repeat the computation for phonon–electron coupling, and show that it is *not* renormalized. Discuss the BCS condition for pairing.

3.4 Landau’s Fermi liquid from a renormalization group viewpoint.

In a Fermi liquid, the infra red behaviour is governed by a trivial fixed point [3,15]. A non Fermi liquid is characterized and governed by non–trivial infra red fixed points, or quasi–fixed points (very slow running).

Landau’s objective was to study the problem of interacting fermions at very low temperatures ($T \ll P_F$). He assumed that the system evolved continuously from the non–interacting limit to the Fermi liquid theory. From a renormalization group point of view this is a trivial (free fermion) fixed point: as one eliminates modes via $k \leq \Lambda$ (the cut–off) one is led to a $1/N_f$ expansion with $N_f \sim k_F/\Lambda$. The Landau (fixed) point is the limit $N_f \rightarrow \infty$. However, if there are relevant operators, they can lead to deviations from Landau’s fixed point, and hence from Fermi liquid behaviour. Theories which are known to deviate in this way are BCS theory, statistical gauge field theories, in whose presence Coulombic interactions are modified, and gauge field theories themselves.

Deviations from Fermi liquid behaviour have been observed in the normal phase of high– T_c cuprates. It may therefore be possible to describe these materials using a model governed by a non–trivial (quasi–) fixed point, e.g. QED₃ (see sections 4 ff.).

In Fermi liquid theory, the low energy excitations are fermions with a fermi surface. The current carrying excitations are quasiparticles, which have width

$$\Gamma \sim E \left(\frac{E}{E_F} \right)$$

where E is some typical energy scale or temperature, and E_F is the Fermi energy, characteristic for electrons. In a renormalization group sense the Fermi liquid theory has no relevant or marginal interactions. There are three main ways in which a model can differ from normal Fermi liquid behaviour:

- (i) Marginal interactions:

$$\Gamma \sim E$$

which implies that the electrical resistivity (see section 6.3.1) in the normal phase of a superconductor is linear in the temperature instead of quadratic:

$$\rho \sim T.$$

- (ii) BCS instabilities (in the superconducting phase of a superconductor).
- (iii) Relevant perturbations: e.g. deformations of the Fermi surface. Note that the issue of naturalness plays a rôle here: the deformations of the Fermi surface would have to be fine–tuned otherwise a small change in (e.g.) the doping would change all the relevant parameters.

Appealing to experiment [16,17], the non Fermi liquid behaviour in the high– T_c shows remarkable stability up to $T \simeq 600K$: this excludes (iii) by the fine–tuning argument [18]. With this phenomenology in mind, it has been argued that the best method is the first, that of marginal interactions.

3.5 Concluding remarks.

The basic features of the renormalization group approach to the Fermi surface are as follows:

- Measure momenta from the Fermi surface.
- Define quasiparticles (“dressed excitations”) with the correct renormalization group scaling behaviour.
- Write down the most general low energy effective–theory interaction terms allowed by the symmetries of the full theory.
- Compute the scaling behaviour of the interactions as the energy scale goes to zero, considering quantum corrections (loops).
- Identify the marginal and relevant interactions: these are important for infra red physics.
- Naturalness requirement for effective field theories: masses must be constrained to vanish by symmetries or else unnatural fine tuning is required to cancel masses which will naturally be $\mathcal{O}(\Lambda)$. Deformations of the Fermi surface are relevant parameters, and act like a masses, and therefore must also satisfy the *naturalness* requirement.

4 Lecture II (i): Non–Trivial Infra Red Structure in QED₃.

As an application of some of the ideas presented in the first lecture, a large- N_f , renormalization group improved approach to the study of U(1) gauge theory in three dimensions is presented. The study of systems with a Fermi surface leads to a natural interpretation of the physics of these gauge theories in terms of a “flow in theory space,” associated with the running of the effective coupling $1/N_f$.

Renormalization group improved Dyson–Schwinger computations in three dimensional U(1) gauge theories have revealed the existence of non–trivial infra red behaviour as a result of fixed point structure [8,19,20]; see also reference [21]. This fixed point structure may explain the non Fermi liquid behaviour of high- T_c superconductors in their normal phase, or the physics of planar antiferromagnets.

In models with a Fermi surface, renormalization group treatments show that the effective coupling $1/N_f$ is related to the (inverse of the) area of the Fermi surface (cf. section 3.2, relation (3.16))

$$\frac{1}{N_f} \longleftrightarrow f \left(\frac{\Lambda}{P_F} \right).$$

If the infrared fixed point in the theory is trivial, then, $1/N_f \rightarrow 0$ and the system is characterized by a large Fermi surface. If on the other hand, there is a running of N_f such that there is no cutoff in the growth of the effective coupling in the infrared, then in the deep infra red the Fermi surface will reduce to a point (a truly relativistic model) as the effective coupling $1/N_f$ runs to infinity. If however, as in QED₃, there exists a non–trivial infra red fixed point, then in the deep infra red, the effective coupling is driven to a finite value and the Fermi surface contracts to a small pocket. If the deformations of the Fermi surface are small then all points on the Fermi surface are equivalent, and one can linearize about a specific point; this facilitates the use of a relativistic model, which captures the essential qualitative features. The relativistic model is the correct one for describing excitations about the nodes of a d –wave superconducting gap. Such d –wave gaps are known to characterize the physics of high temperature superconductors [22]. If we apply the slave–fermion spin–charge separation hypothesis (see section 6.3.2) then the charged excitations about the nodes correspond to Dirac–like fermions, defining a nodal liquid. The study of three dimensional U(1) gauge theories in the normal (chirally symmetric) phase, where the fermions are massless, serves therefore as a pilot theory for the quantitative study of the nodal liquid systems and their possible deviations from Fermi liquid behaviour due to the non–trivial infra red structure to be discussed below. Looking at excitations beyond such d –wave nodes is a non–relativistic problem. As far as normal phase physics is concerned, however, the arguments at the end of section 3.2 imply that the dominant interactions are among the excitations that lie close to one another and therefore the use of relativistic field theory models may prove to be qualitatively correct as far as deviations from Fermi liquid behaviour are concerned. With this in mind, for the rest of this lecture attention will be restricted to the study of relativistic gauge field theory models.



Figure 4: Schematic form of the Dyson–Schwinger equation for the full fermion propagator. Blobs indicate full non-perturbative quantities.

A phenomenologically important model for the superconducting phase of high- T_c cuprates is τ_3 -QED₃: a U(1) gauge theory with the gauge coupling e replaced with

$$e \mapsto e\tau_3$$

so that there are two fermion sectors which couple to the gauge field with opposite sign:

$$S_{\tau_3}^{\text{INT}} = \int d^3x \bar{\Psi} (e\tau_3 \not{\partial}) \Psi. \quad (4.1)$$

The two fermion sectors correspond to the antiferromagnetic sub-lattice structure of the underlying condensed matter model [23]. For the normal phase which will be the topic of this lecture the sub-lattice structure of the underlying model is not important and from now on it will be ignored. The resulting theory therefore will be ordinary QED₃.

It should be noted in passing that the non-trivial fixed point in QED₃ that we find in our analysis [8, 19] can be compared with the ultra violet fixed point in the the three dimensional Thirring model [24]. There is the interesting possibility that there exists a weak–strong coupling (IR \longleftrightarrow UV) duality which maps between the models.

In the following sections a study of the infra red fixed point structure of a strongly coupled U(1) gauge theory in three dimensions is presented. The non-trivial infra red fixed point structure found is a *non-perturbative* effect, and will be analysed using a large- N_f Dyson–Schwinger treatment. This method is quite distinct from conventional Gell–Mann–Low renormalization group analyses; it is closer in spirit to the Wilsonian effective action method discussed in the first half of the lectures.

4.1 Zero temperature analysis of QED₃.

The three dimensional model considered is a U_S(1) gauge theory of N_f 4-component fermion flavours interacting with a statistical gauge field a_μ .

$$S = \int d^3x \left(\frac{1}{4e^2} F_{\mu\nu}^2(a) + \sum_{i=1}^{N_f} \bar{\Psi}_i (i \not{\partial} + \not{a}) \Psi_i + \mathcal{L}_{\text{GF}}(\xi) \right), \quad (4.2)$$

where the covariant gauge fixing term is given by

$$\mathcal{L}_{\text{GF}}(\xi) = -\frac{1}{2\xi} (\partial_\mu a^\mu)^2. \quad (4.3)$$

For most of what follows, Landau gauge will be used ($\xi \rightarrow 0$).

In the large- N_f limit, a Dyson–Schwinger equation treatment can be used; the limit is taken in such a way that

$$\alpha \doteq \frac{e^2 N_f}{8} = \text{constant}; \quad (4.4)$$

the resulting Dyson–Schwinger equations are shown schematically in figures 4 and 5. The Dyson–Schwinger equation for the gauge propagator contains only graphs of leading order in $1/N_f$: typical graphs not appearing in the resummation are indicated in figure 6.



Figure 5: Schematic form of the Dyson–Schwinger equation for the gauge field propagator: only leading terms in $1/N_f$ have been kept.



Figure 6: Typical graphs not appearing (to leading order in $1/N_f$) in the resummed Dyson–Schwinger equation for the gauge propagator (figure 5).

To proceed, an *ansatz* for the fermion propagator is constructed, and then the Dyson–Schwinger equations are solved for the functions appearing therein:

$$\begin{aligned}
 S_F^{-1}(p) &= -i(A(p) \not{p} + B(p)); \\
 A(p) &= \text{Wavefunction renormalization,} \\
 B(p) &= \text{Gap function.}
 \end{aligned} \tag{4.5}$$

The mass gap is given by

$$M \equiv \lim_{p \rightarrow 0} \frac{B(p)}{A(p)}, \tag{4.6}$$

and the normal phase is such that $M = 0$. Solving the Dyson–Schwinger equations leads to coupled integral equations for A and B :

$$\begin{aligned}
 A(p) &= 1 - \frac{\alpha}{\pi^2 N_f} \frac{1}{p^3} \int_0^\infty dk \frac{k A(k) G(p^2, k^2)}{k^2 A^2(k) + B^2(k)} \mathcal{I}_1(k, p; \alpha); \\
 B(p) &= \frac{\alpha}{\pi^2 N_f} \frac{1}{p} \int_0^\infty dk \frac{k B(k) G(p^2, k^2)}{k^2 A^2(k) + B^2(k)} \mathcal{I}_2(k, p; \alpha),
 \end{aligned} \tag{4.7}$$

with the integrals given by:

$$\begin{aligned}
 \mathcal{I}_1(k, p; \alpha) &= \alpha^2 \ln \left[\frac{k+p+\alpha}{|k-p|+\alpha} \right] - \alpha (k+p - |k-p|) \\
 &\quad - \frac{1}{\alpha} |k^2 - p^2| (k+p - |k-p|) + 2kp \\
 &\quad - \frac{1}{\alpha^2} (k^2 - p^2) \left\{ \ln \left[\frac{k+p+\alpha}{|k-p|+\alpha} \right] - \ln \left[\frac{k+p}{k-p} \right] \right\}; \\
 \mathcal{I}_2(k, p; \alpha) &= 4 \ln \left[\frac{k+p+\alpha}{|k-p|+\alpha} \right].
 \end{aligned} \tag{4.8}$$

In fact these integrals are heavily damped for $k > \alpha$, and α can be thought of as an effective (dynamically generated) ultra violet cut-off. This dynamical scale arises directly from the super-renormalizability of QED₃.

The momentum-dependent parts of the full vertex have been written in terms of the function G :

$$\Gamma_\mu(p^2, k^2) = \gamma_\mu G(p^2, k^2), \tag{4.9}$$

and this function has to be determined from the Ward–Takahashi identities.

A common *ansatz* for the vertex is to write the function G in terms of the wavefunction renormalization A :

$$\Gamma_\mu(p^2, k^2) = \gamma_\mu G(p^2, k^2) = \gamma_\mu A^n(k). \quad (4.10)$$

The value of n is a parameter; the Ward–Takahashi identity can in principle be used to determine n but there exist kinematical singularities $1/q^2$ as $q \rightarrow 0$ in the identity. Here n will be kept undetermined for the moment, and the issue of the Ward–Takahashi identity will be ignored.

There are two important features of the above system of integral equations [25, 26]:

- (i) An infra red cutoff ε is required.
- (ii) There exists a critical flavour number $N_c = N_c(\varepsilon)$. As $\varepsilon \rightarrow 0$, so $N_c \rightarrow \infty$.

The infra red cut-off can be related to any convenient scale, for example the temperature, the size of the system, etc.

At low momenta $p \ll \alpha$ a non-zero gap function can be found leading to a finite dynamical mass which breaks chiral symmetry. In particular, for $A = 1$ and in Landau gauge the mass is found to be

$$M \sim \mathcal{O}(1) \alpha e^{-2\pi/\sqrt{(N_c/N_f-1)}}, \quad (4.11)$$

and for $N_f < N_c$ there is a chiral symmetry–breaking dynamical mass.

This analysis is applicable for momenta in the region

$$M \ll p \ll \alpha.$$

In realistic systems (i.e. field theories describing microscopic systems with Fermi surfaces) there is another scale in the problem, namely P_F . Big Fermi surfaces imply large- N_f as modes are eliminated to pass from lattice to continuum limit(s).

In these condensed matter models the hierarchy of scales is as follows:

$$M \ll p \ll \alpha \ll P_F, \quad (4.12)$$

and the ultra violet region in which there is no mass generation is such that $k \in (\alpha, P_F)$. In this regime

$$N_f^{-1} \sim \alpha/P_F \rightarrow 0.$$

This is to be contrasted with QED₃ where α behaves like an ultra violet cut-off, and the kernels of the Dyson–Schwinger equations die off quickly above this scale: there is no dynamical mass generation above α in QED₃.

In the low momentum region the kernels of equations (4.7) can be expanded in powers of p/α and k/α to obtain

$$\begin{aligned} A(p) &= 1 - \frac{g_0}{3} \int_\varepsilon^\alpha dk \frac{k A^{n+1}(k)}{k^2 A^2(k) + B^2(k)} \left[\left(\frac{k}{p} \right)^3 \theta(p-k) + \theta(k-p) \right], \\ B(p) &= g_0 \int_\varepsilon^\alpha dk \frac{k A^n(k) B(k)}{k^2 A^2(k) + B^2(k)} \left[\frac{k}{p} \theta(p-k) + \theta(k-p) \right]. \\ g_0 &\equiv \frac{8}{\pi^2 N_f} \end{aligned} \quad (4.13)$$

This system can be studied in the following three momentum regions:

- $p \ll \alpha$ Low energies: Dynamical mass generation and chiral symmetry breaking;
- $p \sim \alpha$ Intermediate scales: wavefunction renormalization in the normal phase;
- $p \gg \alpha$ Very high energies: super-renormalizability at work.

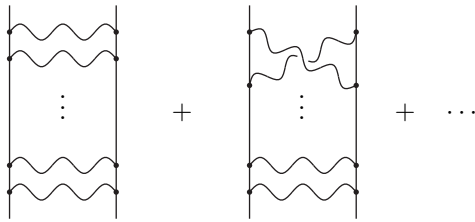


Figure 7: The ladder graphs important in the $p \gg \alpha$ region.

The results of the renormalization group enhanced Dyson–Schwinger analysis described above lead to the concept of a “slow running” of N_f which can be thought of as a flow in theory space [8,19]. As will be shown in subsequent sections, the dimensionless coupling g_0 in equation (4.13) will be renormalized to a running coupling $g_R(p)$. Specifically, it will be shown that in the infra red region $p \ll \alpha$ the following scaling holds:

$$g_R \doteq \frac{8}{\pi^2 N_f(\alpha, p)} \sim \left(\frac{p}{\alpha}\right)^{-\gamma}, \quad (4.14)$$

where γ is determined in the subsequent analyses. In the context of condensed matter models with a Fermi surface of size P_F , this result is to be interpreted as determining the function $f(\Lambda/P_F)$ in relation (3.16), associated with the size of the Fermi surface fundamental cell, provided that one works in a regime where $P_F \sim \alpha$ and the rôle of the scale Λ is played by the momentum p . Note that this regime should not be confused with the ultra violet regime $\alpha \ll P_F$, which should correspond to the Landau fixed point.

The presence of the (spontaneous) infra red scale ε changes the situation at low energies: there exists non-trivial (quasi-) fixed point structure. The fixed point is called “quasi-fixed” for the infra red cut-off must be removed for the fixed point to be determined. The computations show non Fermi-liquid behaviour, and it is most likely that there is a cross-over between the two phases (i.e. not a phase transition).

4.2 Studies in the $p \gg \alpha$ region.

In the very high energy region, the gauge boson polarization tensor behaves as

$$\lim_{p \rightarrow \infty} \Pi(p) \sim \frac{\alpha}{8p} \rightarrow 0,$$

and only ladder graphs like those in figure 7 are important [8]; this is called the quenched or ladder approximation.

The wavefunction renormalization in covariant gauge (see equation (4.3) with arbitrary ξ) is given by

$$A(p) = 1 - \frac{1}{3p^2} \text{Tr} [\not{p} B(p)], \quad (4.15)$$

and the gap function is split into two parts, dependent respectively on the longitudinal and transverse parts of the vertex [27]:

$$B(p) = B^L(p) + B^T(p). \quad (4.16)$$

Now the trace can be evaluated ($x = p^2$), and it is found that the transverse part vanishes:

$$\frac{1}{3} \text{Tr} [\not{p} B^T(p)] = \frac{e^2}{8\pi^2} \int_{\varepsilon^2}^{\Lambda^2} dy \frac{y^{1/2} A(y)}{y A^2(y) + B^2(y)} x T(x, y), \quad (4.17)$$

for it is a rigorous result that $T(x, y)$ vanishes identically:

$$T(x, y) = I_0^0(x, y) - (x - y)^2 I_2^0(x, y);$$

where

$$I_n^m(x, y) = \int_0^{2\pi} d\theta \frac{\sin \theta \cos^m \theta}{(x + y - 2\sqrt{xy} \cos \theta)^2}.$$

Hence only the longitudinal part of the vertex contributes through B^L in quenched QED₃: again in covariant gauge,

$$A(p) = 1 + \frac{e^2}{8\pi^2} \int_{\varepsilon^2}^{\Lambda^2} dy \frac{y^{1/2} A(y)}{y A^2(y) + B^2(y)} L(x, y), \quad (4.18)$$

with

$$L(x, y) = \frac{\xi}{x} [(x + y)I_1^0(x, y) - (x - y)^2 I_2^0(x, y)]. \quad (4.19)$$

So in Landau gauge ($\xi \rightarrow 0$) in quenched QED₃ there is no wavefunction renormalization:

$$A_{\text{quenched}}(p) = 1,$$

and there is no renormalization of the effective flavour number N_f . This corresponds to a trivial fixed point of the β -function: in the current model, this occurs at high energies, and demonstrates that the fermions are *asymptotically free* (for an appropriate choice of the vertex consistent with gauge invariance, and for $N_f \rightarrow \infty$).

4.3 Studies in the $p \lesssim \alpha$ regions: the wavefunction renormalization.

In the low and intermediate momentum regions, the wavefunction renormalization deviates from unity, and becomes important for the physics of both the normal phase and for dynamical mass generation.

In Landau gauge, the wavefunction renormalization is

$$A(p) \simeq 1 + \mathcal{O}\left(\frac{1}{N_f}\right), \quad (4.20)$$

and so is ignored in a resummed $1/N_f$ approximation. With this prescription it can be shown that there exists a critical flavour number, N_c such that chiral symmetry is dynamically broken for $N_f \leq N_c$ [28]. Note, however, the criticisms of references [29, 30].

The precise form of the wavefunction renormalization from the $1/N_f$ resummed graphs is as follows, which shows the critical exponent (anomalous dimension) indicative of the fixed point structure:

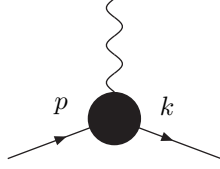
$$A(p) \simeq \left(\frac{p}{\alpha}\right)^{8/3\pi^2 N_f}. \quad (4.21)$$

So for $p \sim \alpha$ and in Landau gauge $A(p) \rightarrow 1$, but for $p \ll \alpha$ the wavefunction renormalization is relevant for dynamical mass generation. $A(p)$ has logarithmic scaling corrections: there is no critical flavour number, and chiral symmetry breaks for all $N_f < \infty$. However this result is not free of ambiguities, for there remain the problems of the choice of vertex and of satisfying the Ward–Takahashi identities.

Regardless of the (non-) existence of a critical flavour number, the issue of the wavefunction renormalization is crucial, and will be studied in more detail in the rest of the lectures.

4.4 The vertex *ansatz* and the wavefunction renormalization.

In a complete treatment, the vertex *ansatz* would be determined by gauge invariance, through the Ward–Takahashi identity, figure 8. This is in general intractable, for the Ward–Takahashi identity requires the full fermion two–point function for its solution; in fact, the situation is worse, for there are kinematical singularities in the identity as $p - k \rightarrow 0$. In practice, then, vertex *ansätze* are constructed which it is hoped capture the essential features of the full vertex.



The diagram shows a central black circle representing a vertex. A wavy line enters from the top. Two straight lines enter from the bottom-left and bottom-right, labeled with momenta p and k respectively.

$$(p - k)_\mu \Gamma^\mu(k, p) = iS_F^{-1}(k) - iS_F^{-1}(p)$$

Figure 8: The Ward–Takahashi Identity.

4.4.1 Simplified treatments.

First, the simplified treatments of references [8, 25] are discussed which relate the vertex to the wavefunction renormalization via a parameter n which is to be determined:

$$\Gamma_\mu(p^2, k^2) = \gamma_\mu A^n(k). \quad (4.22)$$

The Pennington–Webb vertex [29], which does satisfy the Ward–Takahashi identity as $q = p - k \rightarrow 0$, has $n = 1$.

The Dyson–Schwinger equations lead to a definition of an effective “running” coupling by the following procedure:

1. Use a vertex *ansatz*.
2. Apply the bifurcation method (set $B(p) = 0$ in the denominator of the kernel) to the integral equation for $A(p)$.
3. Substitute the solution for $A(p)$ into the equation for $B(p)$.
4. Require running coupling [31]:

$$\begin{aligned} \frac{e^2}{\alpha} \doteq g_R &\equiv \frac{g_0}{A(p, \varepsilon)}; \\ g_0 &\equiv \frac{8}{\pi^2 N_f} \implies g_R = \frac{8}{\pi^2 N_f(\alpha, p, \varepsilon)}. \end{aligned} \quad (4.23)$$

To solve the system of Dyson–Schwinger equations it is essential to introduce an infra red cut–off (see section 4.5) and use a Wilsonian renormalization group approach. As seen in equation (4.23) this leads to a renormalization of the flavour number N_f , and hence a renormalization group flow in theory space.

4.4.2 More refined treatments.

Better treatments have been made of the vertex issue for the wavefunction renormalization [21, 32]: they involve solving the Dyson–Schwinger system of equations self–consistently including the gauge boson polarization, without an infra red cut–off, and with various vertex *ansätze*:

$$\Pi(q) = e^2 N_f \int \frac{d^3 k}{(2\pi)^3} \left(2k^2 - 4k \cdot q - \frac{6(k \cdot q)^2}{q^2} \right) \frac{A(k)}{k^2 A^2(k) + B^2(k)} \frac{A(p) \mathcal{F}(A(p), A(k), A(q))}{p^2 A^2(p) + B^2(p)}, \quad (4.24)$$

where $q = p - k$.

The vertex *ansätze* are as follows [32]

$$\Gamma_\mu = \gamma_\mu \mathcal{F}(A(p), A(k), A(p - k)) : \quad (4.25)$$

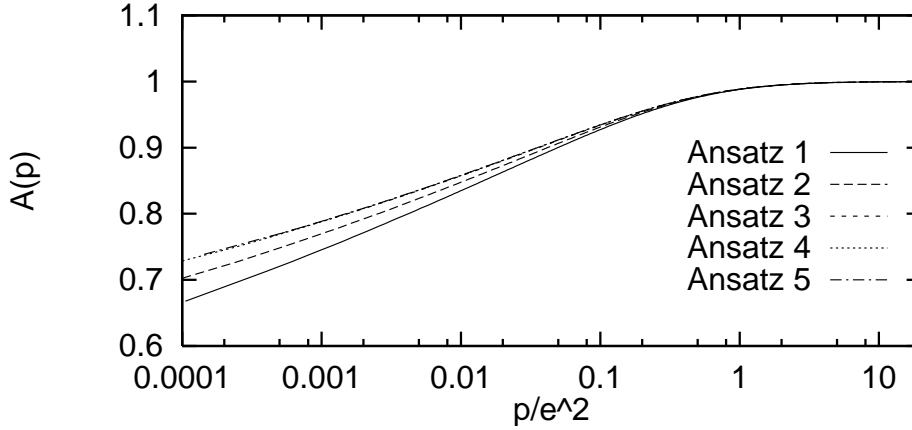


Figure 9: The wavefunction renormalization as a function of the momentum for the five *ansätze* (4.26). (After Maris, [32].)

1. Bare vertex : $\mathcal{F} = 1$.
 2. $\mathcal{F} = \frac{1}{2} [A(p) + A(k)]$
 3. $\mathcal{F} = \frac{A(p) A(k)}{A(p-k)}$
 4. $\mathcal{F} = \frac{1}{4} [A(p) + A(k)]^2$
 5. $\mathcal{F} = A(p) A(k)$.
- (4.26)

The first and second of these are the only physically motivated vertex *ansätze*; the last is motivated by computational simplicity, and the others are included to determine how much the vertex choice affects the results [32]. The third *ansatz* yields

$$\Pi(q) \sim \frac{\alpha q}{A(q)}$$

like the $n = 1$ *ansatz* described earlier.

The results of this analysis of the vertex choice are unfortunately inconclusive (figure 9), though there is suggestion of the existence of non-trivial infra red structure, comparable with the critical behaviour described earlier (equation (4.21)). The behaviour shown in figure 9 is modified in the presence of an infra red cut-off, as will be described in the next section.

4.5 The infra red cut-off.

There are two main methods for introducing an infra red cut-off to the system of equations (4.7):

1. Wave function renormalization with a momentum space infra red cut-off ε directly as a lower limit of integration. Using the bifurcation method:

$$A(p, \varepsilon) = 1 - \frac{\alpha}{\pi^2 N_f} \frac{1}{p^3} \int_{\varepsilon}^{\infty} dk \frac{\mathcal{I}(p, k)}{k}; \quad (4.27)$$

practically speaking, the upper limit of integration is α for the integrand is heavily damped above this scale. The variable infra red scale should be compared with the variable ultra violet scale in a Wilsonian renormalization group approach.

2. Wavefunction renormalization with covariant infra red cut-off δ . Again using the bifurcation method:

$$A(p, \delta) = 1 - \frac{\alpha}{\pi^2 N_f} \frac{1}{p^3} \int_0^{\infty} dk \frac{k \mathcal{I}(p, k)}{k^2 + \delta^2}, \quad (4.28)$$

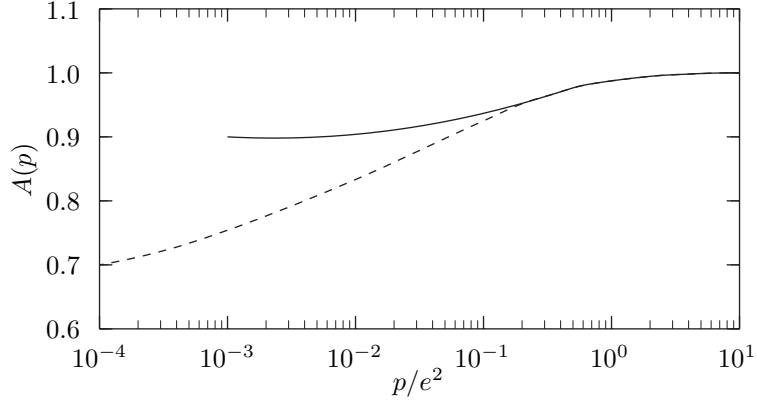


Figure 10: Schematic representation of the wavefunction renormalization as a function of the momentum in the presence of an infra red cut-off $\delta = 0.1$ (continuous curve). The dashed curve indicates the behaviour with no infra red cut-off from figure 9.

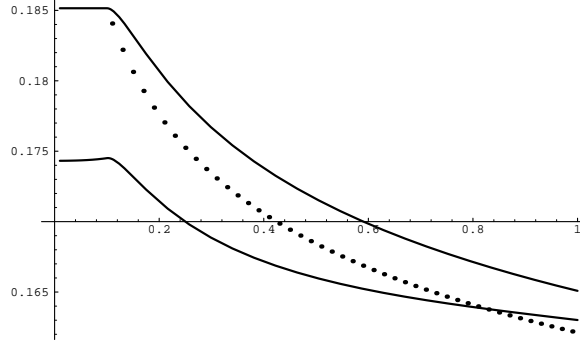


Figure 11: The renormalized coupling (ordinate) in the normal phase as a function of momentum (abscissa) in the presence of a momentum space infra red cut-off ε for different computations of the renormalized coupling. Here $\varepsilon = 0.1$, $\alpha = 1$ and $N_f = 5$.

where again the upper limit is effectively α . This covariant cut-off is similar to the contribution to the plasmon mass in finite temperature condensed matter models [33].

The wavefunction renormalization as a function of momentum is shown schematically in figure 10. This should be compared with the dependence without infra red cut-off, figure 9.

When these infra red cut-offs are removed, neither method gives firm results for the infra red fixed point. As $\varepsilon \rightarrow 0$ the truncated vertex *ansatz* plays an important rôle and the fixed point cannot be identified. The removal of δ is not smooth; this should be compared with the discontinuities as $T \rightarrow 0$ in the plasmon mass model mentioned above [33], and again, the fixed point cannot be identified.

4.5.1 Graphical results.

The following four figures are from reference [20]; results are presented for $\alpha = 1$ and $N_f = 5$.

In figure 11 the renormalized coupling (4.23) is plotted as a function of the momentum in the presence of a momentum space infra red cut-off ε : the upper continuous line is the analytic result [20]

$$g_R = \begin{cases} g_0 / \left(1 - \frac{g_0}{9} + \frac{g_0}{9} \left(\frac{p}{\alpha} \right)^3 + \frac{g_0}{3} \ln \left(\frac{p}{\alpha} \right) \right) & \varepsilon < p < \alpha \\ g_0 / \left(1 + \frac{g_0}{3} \ln \left(\frac{\varepsilon}{\alpha} \right) \right) & 0 < p < \varepsilon \end{cases} . \quad (4.29)$$

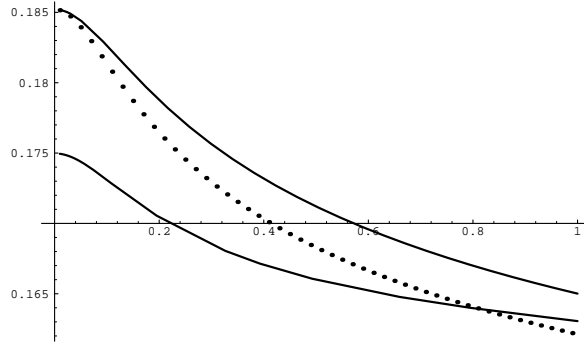


Figure 12: The renormalized coupling in the normal phase as a function of momentum in the presence of a covariant cut-off δ for different computations of the renormalized coupling (4.23). Here $\delta = 0.1$, $\alpha = 1$ and $N_f = 5$.

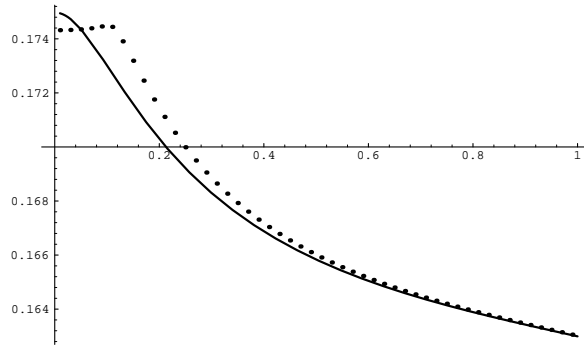


Figure 13: The renormalized coupling as a function of momentum for different types of infra red cut-off. The dotted and continuous curves respectively show $g_R(p, \varepsilon = 0.1)$ and $g_R(p, \delta = 0.1)$. Again, $\alpha = 1$ and $N_f = 5$.

The dotted curve is a crude approximation [25]:

$$g_R = \begin{cases} g_0 / \left(1 + \frac{g_0}{3} \ln \left(\frac{p}{\alpha}\right)\right) & \varepsilon < p < \alpha \\ g_0 / \left(1 + \frac{g_0}{3} \ln \left(\frac{\varepsilon}{\alpha}\right)\right) & 0 < p < \varepsilon \end{cases} . \quad (4.30)$$

Finally, the lower continuous curve is the exact (numerical) solution of equation (4.23).

In figure 12 the same results are presented but for a covariant type cut-off δ . The upper continuous curve corresponds to the analytic solution

$$g_R = g_0 / \left(1 - \frac{g_0}{9} + \frac{g_0}{3p^2} \delta^2 - \frac{g_0}{3p^3} \delta^3 \tan^{-1} \left(\frac{p}{\delta}\right) + \frac{g_0}{6} \ln \left(\frac{p^2 + \delta^2}{\alpha^2 + \delta^2}\right)\right), \quad (4.31)$$

while the dotted curve corresponds to the crude approximation

$$g_R = g_0 / \left(1 + \frac{g_0}{6} \ln \left(\frac{p^2 + \delta^2}{\alpha^2 + \delta^2}\right)\right). \quad (4.32)$$

Again, the lower continuous line is the numerical solution of equation (4.23).

A comparative study of the two types of infra red cut-off is shown in figures 13 and 14. In the first is a direct comparison of the running of the coupling with p and the two infra red cut-offs (the dotted line is for the momentum space cut-off $\varepsilon = 0.1$). The second is an indication of how the coupling behaves as the cut-off is removed in the two schemes: the coupling is shown as a function of the cut-off, $g_R(p = x, x)$ is

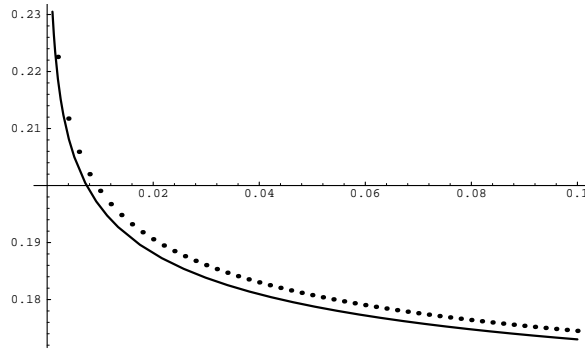


Figure 14: The renormalized coupling as a function of the infra red cut-off. The dotted and continuous curves respectively show $g_R(p \sim \varepsilon, \varepsilon)$ and $g_R(p \sim \delta, \delta)$. Clearly the cut-offs cannot be removed smoothly.

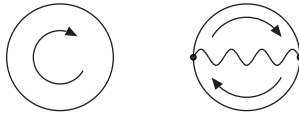


Figure 15: The vacuum graphs in the Wilsonian effective action.

plotted against x , where $x \in \{\varepsilon, \delta\}$ (the dotted curve is for ε). It is clear that neither cut-off can be removed smoothly.

4.5.2 Remark: generic Wilsonian renormalization approach to U(1) gauge theory.

The loops in the Wilsonian effective action (see figure 15) contain circulating momenta which are cut off at M_0 from above and at μ from below. The ultra violet scale M_0 is held fixed and μ is varied in the infra red. For graphs with external lines, terms with external momenta $p < \mu$ are dropped.

If there exist massless states in the theory then it is tricky to determine the infra red behaviour in this approach (c.f. difference between Wilsonian and one-particle irreducible effective actions). The Wilsonian action is finite but there is running $\sim \ln(p/M_0)$. In the presence of an infra red cut-off there is extra running in the infra red with physical consequences. Such gapless fermionic excitations exist in the normal phase of (high- T_c) superconductors.

This behaviour will persist in the Dyson-Schwinger equations obtained from the effective action. This approach can be applied to investigate infra red (quasi-) fixed point structure and deviations from Fermi liquid behaviour in theories with fermions.

4.6 Composite operator effective potential approach.

The computations presented so far have all been for a $1/N_f$ resummed Dyson-Schwinger equation technique, substituting *ansätze* for the vertex and fermion propagator. It is natural to ask whether the infra red structure found is simply an artifact of the approximations and the method. The composite operator effective potential approach yields a partial answer to this question [34]. This approach can be used to investigate the generality of the fermion *ansatz*, at least to leading order in $1/N_f$. Whether the structure is a direct result of the $1/N_f$ truncation is discussed in section 5.

The system of Dyson-Schwinger equations for a theory can in principle be derived from a composite operator effective action [35] via a well-defined minimization technique. If the *ansätze* were put straight into the effective action the same minimization technique could be used to derive the integral equations for the functions appearing therein. Experience in other work [36] has shown that overly restrictive *ansätze* lead to

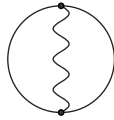


Figure 16: Graph contributing to V_2 up to two-loop level.

differences between Dyson–Schwinger type approaches and the results of composite operator effective action computations.

The composite operator effective action is a generalization of the conventional (quantum) effective action: it is dependent not only on possible vacuum expectation values of the quantum fields (as with the conventional effective action) but also possible vacuum expectation values of composite operators built from the fields. The simplest composite operator effective action is dependent on the expectation value of the two-point function: for QED₃ we are interested in probing the propagator *ansatz* so this will be sufficient. This simplest composite operator effective action is the double Legendre transform of the generating functional for connected Green’s functions. The composite operator effective potential V is then defined directly from the composite operator effective action Γ by removing a factor of the space–time volume:

$$V \int d^D x = -\Gamma. \quad (4.33)$$

For N_f –flavour QED₃ the series expansion for the composite operator effective potential in momentum space is

$$\begin{aligned} V[S_F, D] &= iN_f \int \frac{d^3 p}{(2\pi)^3} \text{tr} \{ \ln [S_F^{-1}(p) S_0(p)] + S_0^{-1}(p) S_F(p) - 1 \} \\ &- \frac{i}{2} \int \frac{d^3 p}{(2\pi)^3} \text{tr} \{ \ln [D^{-1}(p) D_0(p)] + D_0^{-1}(p) D(p) - 1 \} \\ &+ V_2[S_F, D]. \end{aligned} \quad (4.34)$$

The functions S_F and D are candidate full non-perturbative two-point functions for the fermions and gauge field respectively, and the subscripts ₀ denote their bare counterparts. To determine the actual (physical) non-perturbative two-point functions for the theory, the effective potential must be minimized with respect to (functional) variations in S_F and D . Here $-V_2$ is the sum of all two-particle irreducible vacuum graphs with propagators set equal to S_F and D and with bare (undressed) vertices. In order to consider more general vertices one would have to consider a “trilocal” effective action (three Legendre transforms) and require that this new object be stationary with respect to variations in the vertex *ansatz* [34].

Truncating the series for V_2 at two-loop level, figure 16, is sufficient to compare with the Dyson–Schwinger method for QED₃. Variation of equation (4.34) with respect to S_F and D yields the Dyson–Schwinger equations for QED₃, which upon substituting the *ansatz* (4.5) gives the equations (4.7) of section 4.1. It has been shown [34] that if one substitutes the *ansatz* (4.5) directly into the composite operator effective potential (4.34) then requiring it to be stationary with respect to (functional) variations in the wavefunction renormalization A and the gap function B yields *the same* integral equations as the first approach.

Since the composite operator effective potential yields the same integral equations (4.7) whether the *ansätze* are put in before or after the functional variation demonstrates explicitly that it is equivalent to the Dyson–Schwinger method for QED₃. The consistency of the two methods is a strong indication that the *ansätze* are sufficiently consistent and general.

4.7 The physical consequences of “slow running.”

The slow running of the coupling constants (relative to naïve expectations) enhances the chiral condensate

$$\langle \bar{\Psi} \Psi \rangle \sim \int^\Lambda dp p B(p). \quad (4.35)$$

If the running of the coupling is slowed down then there is an enhancement of $B(p)$ at low momenta and therefore of the chiral condensate. This is similar to the situation in “walking technicolour” models [37] where the introduction of extra fermionic degrees of freedom due to a specific choice of an enlarged gauge group slows down the running of the pertinent gauge coupling relative to the model with the original gauge group.

When the field theory is applied to superconductivity models the enhanced condensate might affect the measurable parameter Gap/T_c and the size of the coherence length in magnetic superconductors. Also, in the normal phase, where chiral symmetry is unbroken, the critical behaviour in the wavefunction renormalization leads to deviations from Fermi liquid behaviour [19], and also to anomalous electric transport properties, e.g. the resistivity linear in T (the temperature) with $\ln T$ scaling corrections, which behaviour is stable over a large range of temperatures (see section 6). The critical behaviour in the wavefunction renormalization also modifies the normal critical behaviour (i.e. the critical exponents) in these models.

4.8 Exercises.

4.8.1 The Dyson–Schwinger equations.

Derive the equations (4.7) from the Dyson–Schwinger equations for QED₃ to leading order in $1/N_f$ (figures 4 and 5).

4.8.2 Dyson–Schwinger vs composite operator effective potential.

Show that the equations (4.7) can also be obtained from the composite operator effective potential, equation (4.34).

4.9 Concluding remarks.

- Renormalization group improved Dyson–Schwinger analysis reveals non-trivial infra red fixed point structure in three dimensional U(1) gauge theory. This structure in the low energy limit means that, although QED₃ is super-renormalizable, the degrees of freedom relevant at scales of order the ultra violet cut-off are still applicable in the effective theory for the deep infra red.
- The infra red structure leads to dynamical mass generation and critical behaviour in the normal (chirally symmetric) phase; these are associated with a “slow running” of the effective coupling.
- Critical behaviour for the normal phase of the model affects the wavefunction renormalization

$$A(p) \sim \left(\frac{p}{\alpha}\right)^{8/3\pi^2 N_f}.$$

- The computation of this critical behaviour has been discussed in connexion with a number of vertex *ansätze* and with different infra red cut-offs.
- Slow running of the coupling has physical consequences, such as in the enhancement of the chiral condensate; some of the physical consequences of the critical behaviour of the wavefunction renormalization will be discussed in the last lecture, section 6.

5 Lecture II (ii): Results Beyond Leading Order in $1/N_f$.

A natural question which arises is whether the non-trivial structure observed in the preceding sections is simply an artifact of the truncations (to leading order in $1/N_f$) in the Dyson–Schwinger equations. A partial answer to this question concerning the fermion *ansatz* has already been discussed (section 4.6); some further attempts to answer this question and probe the physics beyond leading order in $1/N_f$ are presented in what follows.

5.1 Non-local gauges.

A treatment of the model beyond $1/N_f$ has been performed recently [21] in which a non-local gauge parameter is introduced which fixes the wavefunction renormalization A to be exactly unity. This approach confirms the earlier results of references [8, 19] for the existence of slow running of the effective coupling in the infra red.

The non-local gauge is defined from the gauge fixing term:

$$\mathcal{L}_{\text{GF}} = -\frac{1}{2}F(a(x)) \int d^3y \frac{1}{\xi(x-y)} F(a(y)), \quad (5.1)$$

where the function F is given by

$$F(a) = \partial_\mu a^\mu.$$

The non-local gauge function ξ is then chosen to ensure $A \equiv 1$ exactly. The results are subsequently transformed back to Landau gauge using the (inverse) Landau-Khalatnikov transformation [38]. Both ε and the covariant δ type infra red cut-offs can be used in the computations and the results compared.

It is found that it is possible to define a running coupling (cf. equation (4.23))

$$\frac{g_{\text{R}}(t)}{g_{\text{R}}(0)} \sim 1 + \frac{\tilde{\xi}(k^2)}{2}; \quad (5.2)$$

$$t = \ln \left(\frac{k}{\mu} \right);$$

where μ is some momentum scale and $\tilde{\xi}(k^2)$ is related to the Fourier transform of the non-local gauge parameter; see equation (5.11).

The momentum space cut-off ε can be removed but when the covariant type of cut-off is used, there exist discontinuities as $\delta \rightarrow 0$ (cf. Landau damping processes at finite temperature mentioned in section 4.5 and in references [33, 39]). In both cases, the infra red fixed point structure and slow running of the coupling found in previous analyses [8, 19] is confirmed.

The running of the coupling with the covariant infra red cut-off δ is described by the β -function:

$$\beta(\tilde{\xi}) = -\frac{d}{dt}\tilde{\xi}(k^2) \sim 4 + \frac{2k^2 + 3\alpha k + 4\delta^2}{k^2 + \alpha k + \delta^2} (\tilde{\xi}(k^2) - 2). \quad (5.3)$$

If $\delta = 0$

$$\beta(\tilde{\xi}) = 3\tilde{\xi}(k^2) - 2 \quad : \quad \tilde{\xi} \xrightarrow{k \rightarrow 0} \frac{2}{3}. \quad (5.4)$$

Compare with $\delta \neq 0$

$$\beta_\delta(\tilde{\xi}) = 4\tilde{\xi}(k^2) - 4 \quad : \quad \tilde{\xi} \xrightarrow{k \rightarrow 0} 1; \quad (5.5)$$

so δ cannot be removed smoothly.

5.2 Infra red critical exponents beyond $1/N_f$ from the non-local gauge.

The suggested form of the wavefunction renormalization in a $1/N_f$ treatment in Landau gauge is [29] (see section 4.3):

$$A(p) \sim \left(\frac{p}{\alpha} \right)^\gamma; \quad p \ll \alpha, \quad (5.6)$$

where the critical exponent is given by

$$\gamma = \frac{8}{3\pi^2 N_f}. \quad (5.7)$$

In the work of reference [20] a non-local gauge is used to verify this form beyond $1/N_f$; the computations are done in a non-local gauge chosen so that $A = 1$ exactly and then the results are transformed back to Landau gauge using the Landau-Khalatnikov transformation [38].

In the normal phase (chiral symmetry unbroken) and in Landau gauge the fermion propagator reads:

$$S_F(p) = [A(p) \not{p}]^{-1} \quad (5.8)$$

and in the non-local gauge in momentum and configuration space

$$\begin{aligned} S'_F(p) &= (\not{p})^{-1}, \\ S'_F(x) &= i \not{x} \frac{\Gamma(3/2)}{2\pi^{3/2} |x|^3}. \end{aligned} \quad (5.9)$$

Now the wavefunction renormalization can be written in terms of the non-local gauge parameter:

$$\begin{aligned} A^{-1}(p) &= -i \int d^3x e^{ip \cdot x} e^{-\Delta(x)} p \cdot x \frac{\Gamma(3/2)}{2\pi^{3/2} |x|^3}; \\ \Delta(x) &\equiv e^2 \int \frac{d^3k}{(2\pi)^3} (e^{-ik \cdot x} - 1) \frac{\tilde{\xi}(k^2)}{k^4 (1 - \Pi(k^2)/k^2)}; \end{aligned} \quad (5.10)$$

the function $\tilde{\xi}(k^2)$ is related to the Fourier transform of the non-local gauge parameter:

$$\tilde{\xi}(k^2) = \xi(k^2) (1 - \Pi(k^2)/k^2), \quad (5.11)$$

and $\Pi(k^2)$ is the vacuum polarization. Since in the non-local gauge $A \equiv 1$ and the trivial (bare) vertex can be chosen while maintaining consistency with the Ward-Takahashi identity, an *exact* expression for the vacuum polarization can be computed:

$$\Pi(k^2) = -\alpha |\vec{k}|. \quad (5.12)$$

In the deep infra red $|\vec{k}| \ll \alpha$ the non-local gauge parameter must satisfy

$$\tilde{\xi}(k^2) = 1 + \frac{1}{(k^2)^2 D_T(k^2)} \int_0^{k^2} dz z^2 \frac{d}{dz} D_T(z); \quad (5.13)$$

with the transverse photon propagator given by

$$D_T(z) = \frac{1}{z + \alpha\sqrt{z}}.$$

The integral can be performed, to yield [20]

$$\tilde{\xi}(k^2) = 2 - 2 \frac{k^2 + \alpha k}{k^2} \left[1 - \frac{2\alpha}{k} + \frac{2\alpha^2}{k^2} \ln \left(1 + \frac{k}{\alpha} \right) \right] \quad (5.14)$$

and the logarithm can be expanded in powers of $k/\alpha \ll 1$ with the result

$$\frac{\tilde{\xi}(k^2)}{k^4 (1 - \Pi(k^2)/k^2)} \simeq \frac{2}{3\alpha} \frac{1}{k^3} - \frac{1}{\alpha^2 k^2} + \frac{6}{5\alpha^3 k}. \quad (5.15)$$

For the evaluation of $\Delta(x)$ the Fourier transform of (5.15) is required:

$$I(x) \equiv \frac{8}{N_f} \int \frac{d^3k}{(2\pi)^3} e^{-ik \cdot x} \left[\frac{2}{3k^3} - \frac{1}{\alpha k^2} + \frac{6}{5\alpha^2} \right]; \quad e^2 = \frac{8\alpha}{N_f}, \quad (5.16)$$

and (see equation (5.10))

$$\Delta(x) = I(x) - I(0). \quad (5.17)$$

The integral needs regularization in the ultra violet and the infra red, so introduce dimensional regulation $d - 3 = \epsilon \rightarrow 0^+$ and the (renormalization group) scale μ :

$$I(x) = \frac{24}{5\pi^2 N_f} \frac{1}{|\alpha x|^2} - \frac{2}{\pi N_f} \frac{1}{|\alpha x|} + \frac{4}{3\pi^2 N_f} \left(\frac{2}{\epsilon} + 2 \ln \left(\frac{1}{|\mu x|} \right) - \gamma_0 \right), \quad (5.18)$$

where γ_0 is the Euler–Mascheroni constant. In order to compute the difference (5.17) the divergences in $I(0)$ must be controlled; for this purpose, $I(0)$ is replaced with $I(1/\alpha)$ [20]:

$$\Delta(x) = I(x) - I(1/\alpha) \sim \frac{24}{5\pi^2 N_f} \left(\frac{1}{x^2} - \alpha^2 \right) - \frac{2}{\alpha\pi N_f} \left(\frac{1}{|x|} - \alpha \right) + \frac{8}{3\pi^2 N_f} \ln \left| \frac{1}{\alpha x} \right|, \quad (5.19)$$

which is independent of the ultra violet renormalization scale μ ; this is a direct consequence of the super-renormalizability of QED₃: there should only be running in the infra red.

Now the infra red behaviour of the wavefunction renormalization can be obtained from equation (5.10):

$$\begin{aligned} A^{-1}(p) &= -i \int d^3x e^{ip \cdot x} p \cdot x \frac{\Gamma(3/2)}{2\pi^{3/2} |x|^3} e^{-\Delta(x)} \\ &\sim \exp \left(\frac{24}{5\pi^2 N_f} - \frac{2}{\pi N_f} \right) \frac{2^\gamma \pi^{3/2} \gamma \Gamma(\gamma/2)}{4\pi \Gamma(\frac{3-\gamma}{2})} \left(\frac{\alpha}{p} \right)^\gamma \quad (p \rightarrow 0); \end{aligned} \quad (5.20)$$

$$\gamma = \frac{8}{3\pi^2 N_f} \quad (5.21)$$

The critical exponent (5.21) confirms the behaviour found in Landau gauge. In the approximate method described above, the prefactor cannot be determined precisely. This prefactor is irrelevant and of order unity, indeed for $N_f = 5$ it has the numerical value 1.007. In section 5.3 a more exact treatment will be described in which the prefactor is determined to be exactly unity. The non-local gauge takes the computation of this critical exponent beyond leading order in $1/N_f$ but confirms the analyses performed to this order. A treatment of the gap function in the non-local gauge yields a critical number of flavours [20]

$$N_c \simeq 4.32 \quad (5.22)$$

which is consistent with $1/N_f^2$ corrections to the normal Landau gauge computations [40].

5.3 Improved computation of behaviour beyond $1/N_f$.

A more refined treatment using the non-local gauge has been performed [41] in which a Dyson–Schwinger type equation for the fermion propagator S is derived in place of the normal equation for S^{-1} . Consider the equations for the fermion propagator in the non-local gauge (S_0 is the free fermion propagator) and in D dimensions:

$$S_{\text{NLG}} = S_0 \quad : \quad i\cancel{\partial} S_0 = \delta^D(x). \quad (5.23)$$

In Landau gauge,

$$\begin{aligned} S_L(x) &= e^{-\Delta(x)} S_{\text{NLG}}(x) = [A(p) \cancel{p}]^{-1}, \\ \Delta(x) &= e^2 \int \frac{d^D k}{(2\pi)^D} (e^{ik \cdot x} - 1) f(k), \\ f(k) &= \frac{\xi(k)}{k^4}. \end{aligned} \quad (5.24)$$

Now, by acting on equation (5.24) with $i\cancel{\partial}$, a Dyson–Schwinger type equation for the fermion propagator in the normal phase can be derived (using the fact that $\Delta(0) = 0$):

$$\begin{aligned} i\cancel{\partial} S_L(x) &= \delta^D(x) - ie^2 S_L \int \frac{d^D k}{(2\pi)^D} \cancel{k} f(k) e^{-ik \cdot x}; \\ \implies A^{-1}(p) &\doteq Z(p) = 1 + e^2 \int \frac{d^D q}{(2\pi)^D} \frac{q \cdot (q-p)}{q^2} f(q-p) Z(q). \end{aligned} \quad (5.25)$$

The solutions of equation (5.25) are as follows [41]

$$Z(p) = 1 - e^2 \int_\epsilon^\Lambda dq Z(q) L(p, q; D),$$

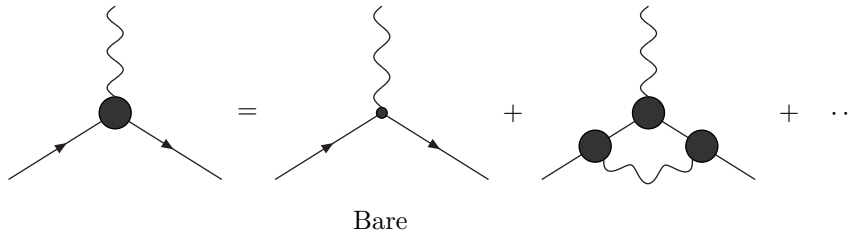


Figure 17: Pinch technique for renormalizing the coupling G from the amputated vertices.

$$\begin{aligned}
 L(p, q; D) &= \frac{q^{D-3}}{2^{D-1} \pi^{(D+1)/2} \Gamma(\frac{D-1}{2})} \int_0^\pi d\theta \sin^{D-2} \theta (pq \cos \theta - q^2) f(\sqrt{(p-q)^2}); \\
 f(k) &= \frac{2}{k^4 + \alpha k^3} - \frac{2}{k^4} \left[1 - \frac{2\alpha}{k} + \frac{2\alpha^2}{k^2} \ln \left(1 + \frac{k}{\alpha} \right) \right].
 \end{aligned} \tag{5.26}$$

Note that in three dimensions $L(q, p; 3)$ is not a symmetric function of its arguments. In the infra red, $k \ll \alpha$ the regularization scale Λ can be taken equal to the effective cut-off α , and the infra red cut-off ε can be taken to zero. In this regime, the equation (5.26) can be solved numerically and analytically using truncated expansions. In the absence of the infra-red cut-off, $\varepsilon \rightarrow 0$,

$$Z(p) = A^{-1}(p) = \left(\frac{p}{\alpha} \right)^{-8/3\pi^2 N_f} \tag{5.27}$$

which is *exact* and the same as the result obtained in reference [20]. It is an open issue as to whether these results are dependent on the type of infra red cut-off, i.e. whether the results are the same if a covariant cut-off is included:

$$\frac{1}{k^2} \mapsto \frac{1}{k^2 + \delta^2}.$$

5.4 An alternative description of running flavour number.

To conclude this section, a comment on the correctness of the effective running coupling inferred above from the special manipulations of the Dyson–Schwinger equations (4.7) in the normal phase.

In field theory the actual running coupling constant is usually defined via the amputated vertex function. There is work currently underway [42] on renormalizing the coupling using a “pinch technique” similar to that used for 4-dimensional QCD [43]. In place of the Dyson–Schwinger equations for the fermion propagator, the Dyson–Schwinger equation for the amputated vertex is investigated (figure 17) and the running of the coupling determined directly. The computations are performed in a large- N_f framework, with $e^2 N_f$ held fixed. Then the dimensionless coupling runs, and generates an effective running of N_f :

$$\left(\frac{e^2}{\alpha} \right)_{\text{ren}} \sim \left(\frac{1}{N_f} \right)_{\text{ren}}. \tag{5.28}$$

The differential equation for the vertex function $G(p)$ is complicated by the presence of infra red cut-offs, and can only be solved numerically at present. The advantage of this method lies in the fact that in determining the vertex directly, the problem of finding vertex *ansätze* satisfying the Ward–Takahashi does not arise.

5.5 Concluding remarks.

- Non-local gauges have been used to probe the infra red physics of three dimensional U(1) gauge theory beyond leading order in $1/N_f$.
- The results have been shown to be consistent with those obtained in conventional $1/N_f$ Dyson–Schwinger treatments. This supports the idea that the non-trivial infra red structure found is not an artifact of the $1/N_f$ truncation.

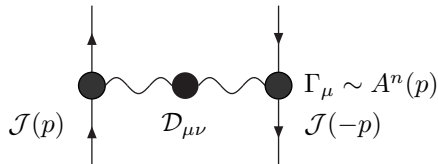


Figure 18: Current–current correlator for the resistivity computation; the wavefunction renormalization affects the resistivity through the vertex.

6 Lecture II (iii): Predictions of Gauge Interactions for Finite Temperature Models.

6.1 The resistivity in gauge field theory models.

In this final part of the lectures the preceding ideas will be applied to a determination of some properties of QED₃ at finite temperature. Attention will be restricted to the predictions of the gauge theory model for the electrical resistivity. The resistivity is defined as the response of a system to a change in external electric field (see section 6.3.1). Formally it is related to the imaginary part of the electric current–current correlator:

$$(\text{Resistivity})^{-1} = (\text{conductivity}) \sim \mathcal{I}m \langle \mathcal{J}_\mu^\Psi(p) \mathcal{J}_\nu^\Psi(-p) \rangle \Big|_{p=0} \propto \mathcal{I}m (A^n(p) \mathcal{D}_{\mu\nu}(p) A^n(p)) \Big|_{p=0}, \quad (6.1)$$

where $A(p)$ is the wavefunction renormalization (which appears here as a result of the vertex *ansatz*, see equation (4.22) and figure 18) and $\mathcal{D}_{\mu\nu}$ is the full gauge field propagator. The current is defined by

$$\mathcal{J}_\mu^\Psi = \frac{\delta S^{\text{eff}}}{\delta A_{\text{ext}}^\mu},$$

with A_{ext}^μ an external electromagnetic potential. As was observed in section 4.4.1, gauge invariance selects the Pennington–Webb vertex with $n = 1$.

The gauge field theory model of superconductivity considered above gives rise to two contributions to the resistivity [8]: the bulk effect of the gauge field and the logarithmic corrections due to the wavefunction renormalization from the vertices (figure 18). We shall review briefly these results in what follows.

To be completely rigorous in deriving equation (6.1) the precise behaviour of the effective action S^{eff} in the infra red is required. However, as will be discussed in section 6.2 there are non–analyticities due to Landau damping [33] which render the infra red limit intractable in the low temperature limit, $T \rightarrow 0$. To circumvent this problem a physical (heuristic) approach will be used, exploiting the spin–charge separation (see sections 6.3.2–6.3.3) in the framework of Ohm’s law. The method used is summarized as follows:

- “Spin–charge separation:” (see section 6.3.2) split the electronic degrees of freedom into holon (charge) and spinon (spin) [44] degrees of freedom (Ψ^\dagger) and (Z_α) respectively

$$C_\alpha = \Psi^\dagger Z_\alpha \quad (6.2)$$

- Assume Ohm’s Law for an external electric field \vec{E} :

$$\mathcal{J}^\Psi = (\text{charge}) \times v_F = \vec{\sigma} \cdot \vec{E}, \quad (6.3)$$

where \mathcal{J}^Ψ is the current for the holon degrees of freedom. Here v_F is the Fermi velocity for holons and is a function of temperature: this temperature dependence arises from non–trivial thermal vacua (in the relativistic limit of antiferromagnets); see section 6.3.3.

The results can be summarized as:

1. The bulk effect of the gauge interactions (if the wavefunction renormalization $A(p)$ is unity) is to give a temperature dependence to v_F of the form

$$v_F \propto T^{-1} \quad \text{for low } T. \quad (6.4)$$

2. For $A(p) \neq 1$

$$\rho \sim \frac{1}{\sigma} \sim T^{1-\mathcal{O}(1/N_f)}. \quad (6.5)$$

The non-trivial infra red structure encoded in the wavefunction renormalization corrects the normal linear behaviour. As was discussed above there are gauges in which the wavefunction renormalization is trivial. The resistivity ρ is physical, and should therefore be gauge invariant: in gauges where the wavefunction renormalization is trivial there are still logarithmic corrections in the resistivity arising from non-trivial structure in the resulting vertex functions.

6.2 The real time formalism and Landau damping.

The action for massive fermions interacting with a $U_S(1)$ statistical gauge field a and an external electromagnetic field A^{em} in three dimensions is

$$S = \int d^3x \bar{\Psi} (i \not{\partial} - e \not{A}^{\text{em}} - g_s \not{a} - M) \Psi; \quad (6.6)$$

it is sufficient to study this model with the statistical gauge field turned off. The one-loop effective action can be computed:

$$\begin{aligned} W^{(1)} &= \frac{ie^2}{2} \int \frac{d^3p}{(2\pi)^3} \tilde{A}_\mu^{\text{em}}(-p) \tilde{\Gamma}^{\mu\nu}(p) \tilde{A}_\nu^{\text{em}}(p); \\ \tilde{\Gamma}^{\mu\nu}(p) &= \int \frac{d^3k}{(2\pi)^3} \text{tr} [\gamma^\mu S_F(k+p) \gamma^\nu S_F(k)]. \end{aligned} \quad (6.7)$$

As an example of non-analyticities near the origin in p -space, consider the odd parity part of $\tilde{\Gamma}$:

$$\begin{aligned} \tilde{\Gamma}_{\text{odd}}^{\mu\nu}(p) &= -2F(p) \epsilon^{\mu\nu\lambda} p_\lambda \\ F(p) &= -iM \int \frac{d^3k}{(2\pi)^3} \frac{1}{[(k+p)^2 - M^2][k^2 - M^2]}. \end{aligned} \quad (6.8)$$

Here the imaginary time formalism is used to compute finite temperature effects: perform an analytic continuation to Minkowski space:

$$p_3 \mapsto -ip_0.$$

The result after such a continuation is (with β the inverse temperature)

$$\begin{aligned} F_\beta(p_0, \vec{p}) &= \frac{M}{4} \int \frac{d^2k}{(2\pi)^2} \left[\frac{n_F(E_k) + n_F(E_{k+p})}{p_0 - E_k - E_{k+p}} - \frac{n_F(E_k) + n_F(E_{k+p})}{p_0 + E_k + E_{k+p}} - \frac{n_F(E_k) - n_F(E_{k+p})}{p_0 - E_k - E_{k+p}} \right. \\ &\quad \left. + \frac{n_F(E_k) - n_F(E_{k+p})}{p_0 + E_k - E_{k+p}} \right], \end{aligned} \quad (6.9)$$

where

$$n_F(E) \doteq \tan \frac{\beta E}{2} = -i [1 - 2n_F(iE)]$$

is the Fermi-Dirac distribution.

The denominators of F have discontinuities along the real axis, which lead to delta functions and contributions to the imaginary parts of the effective action F_β and hence to physical processes, e.g. fermion \leftrightarrow fermion + gauge quantum: Čerenkov processes or (in many body language) *Landau damping*.

$$\delta(p_0 + E_k - E_{k+p}) \quad : \quad E_{k+p} = \left[M^2 + (\vec{k} + \vec{p})^2 \right]^{1/2} \simeq E_k + \frac{\vec{p} \cdot \vec{k}}{E_k}$$

Near the origin of momentum space the δ -function condition leads to

$$p_0 = \frac{\vec{p} \cdot \vec{k}}{E_k} = \vec{p} \cdot \vec{v}_k \quad (6.10)$$

where v_k is the fermion velocity; and there is a discontinuity in the space-like region $p_0 \leq |\vec{p}|$.

There are non-analyticities associated with such processes. The argument in qualitative terms follows. The contribution to the imaginary part of F_β involves angular integrations for both \vec{p} and \vec{k} . But there exists a cut in the p_0 plane which extends from $-|\vec{p}|$ to $|\vec{p}|$. So for $|\vec{p}| \rightarrow \vec{0}$ (which is a relevant limit for the computation of the resistivity, equation (6.1)) there is non-analyticity. It is worth noting in passing that this situation is analogous to the case of BCS superconductivity for $T < T_c$ in a time dependent Ginzburg–Landau theory. This has also been verified by explicit computation [33].

The non-analyticities described above result in a non-local effective action and complicate the situation enormously. A way out of this problem is to use approximate closed expressions for low p and then numerically verify them up to momenta and energies of order of the fermion mass scale in the particular problem. In this way it is possible to construct an effective action that is local for some region of parameter space.

A more physical way out of this problem is to use a heuristic approach involving spin–charge separation in conjunction with Ohm’s law which is the subject of the next subsection.

6.3 Spin–charge separation and resistivity.

6.3.1 Resistivity and Ohm’s law.

Consider the case of QED₃ in the presence of an external electric field \vec{E} corresponding to an electromagnetic potential A_μ^{em} . Starting with the action (6.6) and integrating out all fields but the electromagnetic:

$$\begin{aligned} S &= \int d^3x \bar{\Psi} (i \not{\partial} - \not{a} - e \not{A}_{\text{em}}) \Psi \\ S_{\text{eff}} &= \int d^3x A_{\text{em}}^\mu(p) \mathcal{D}_{\mu\nu} A_{\text{em}}^\nu(-p); \\ \mathcal{D}_{\mu\nu} &= \left(\delta_{\mu\nu} - \frac{p_\mu p_\nu}{p^2} \right) \frac{1}{\vec{p}^2 + \Pi}. \end{aligned} \quad (6.11)$$

The electric current is given by

$$\frac{\delta S_{\text{eff}}}{\delta A_{\text{em}}^i} \equiv \mathcal{J}_i^{\text{el}} \propto E_i(\omega). \quad (6.12)$$

In momentum space the electric field $E_i(\omega)$ is given by ωA_i^{em} . Hence Ohm’s law in a gauge with $A_0^{\text{em}} = 0$ gives the conductivity as [45]

$$\sigma_f = \frac{1}{\vec{p}^2 + \Pi} \Big|_{\vec{p}=\vec{0}}. \quad (6.13)$$

6.3.2 The spin–charge separation formalism.

In the slave fermion spin–charge separation formalism [23, 46] the electron degrees of freedom are split into two parts at each lattice site n of the condensed matter model:

$$C_\alpha^n = \Psi_n^\dagger Z_\alpha^n, \quad (6.14)$$

where Ψ is a spinless electrically charged fermion (hole) and Z_α , $\alpha \in \{1, 2\}$ is a CP^1 magnon which carries the spin part of the degrees of freedom.

There is a constraint of at most one electron per lattice site which is expressed as

$$\Psi_n^\dagger \Psi_n + (Z_n^*)_\alpha (Z_n)_\alpha = 1, \quad (\text{no sum over } n).$$

In view of this, the currents are related by

$$\vec{\mathcal{J}}^\Psi + \vec{\mathcal{J}}^Z = \vec{0}, \quad (6.15)$$

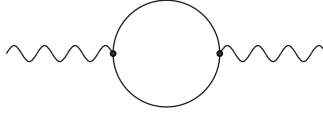


Figure 19: The fermion vacuum polarization contribution to the gauge boson two–point function.

where

$$\vec{\mathcal{J}}^\Psi = \bar{\Psi} \vec{\gamma} \Psi \quad \vec{\mathcal{J}}^Z = Z^* \vec{\partial} Z. \quad (6.16)$$

The movement of the charge carriers is governed by the transport velocity, which is that of the CP^1 gauge fields, i.e. in the relativistic effective field theory. Here v_f plays the rôle of the “speed of light,” insofar as it is a limiting velocity for the low energy excitations.

In order to compute the resistivity we use the phenomenological Ohm’s law:

$$\mathcal{J}^\Psi = \text{charge} \times v_f = \vec{\sigma} \cdot \vec{E}. \quad (6.17)$$

As will be shown next the Fermi velocity v_f is a function of temperature in non–trivial thermal vacua [47]. A non–trivial thermal vacuum arises in finite temperature QED₃ due to fermion vacuum polarization, see figure 19.

6.3.3 Speed of light in non–trivial vacua.

The effective speed of light can be computed [8] from the dispersion relation induced by the fermion vacuum polarization (see figure 19)

$$v_f^{\text{eff}} = \frac{\partial E}{\partial Q}, \quad (6.18)$$

where E is the energy of off–shell gauge bosons (cf. on–shell Landau processes as the main contributions to microscopic resistivity):

$$E^2 \equiv q_0^2 = Q^2 + \Pi(Q, \beta), \quad (6.19)$$

and Π is the thermal vacuum polarization (pertaining to the real part of the effective action). For on–shell gauge bosons the denominator of the propagator vanishes.

An approximate *ansatz* (found to be a good approximation numerically) which qualitatively captures the correct behaviour is [26]

$$\begin{aligned} \Pi(Q, \beta) &\sim \Pi_L \simeq \Pi_T \simeq \left(\frac{\alpha p^2}{64} + 4\omega_\pi^4 \right); \\ p^2 &\equiv p_3^2 + \vec{p}^2 \end{aligned} \quad (6.20)$$

with ω_π the plasmon mass. It is found that this approximate form is applicable over a large temperature range. Then

$$v_f \propto \frac{Q}{T^{3/2}} : \quad Q \longrightarrow \varepsilon_{\text{IR}} \sim \sqrt{(\alpha/\beta)} \propto \sqrt{T}. \quad (6.21)$$

Hence the behaviour of the resistivity is easy to infer from equation (6.17), assuming T –independence of the electric field \vec{E} ,

$$v_f \sim T^{-1} \implies \rho \propto T. \quad (6.22)$$

This type of resistivity response in the bulk is characteristic of a gauge interaction, and strongly suggests that the gauge model correctly describes the physics in these materials. Indeed it is very hard to arrange this behaviour in models with non–gauge interactions.

6.3.4 Logarithmic corrections to the resistivity.

The linear- T behaviour demonstrated above has logarithmic corrections coming from the wavefunction renormalization. To compute these it is only necessary to look at the real parts of the effective action. The Dyson-Schwinger equation for the wavefunction renormalization at finite temperature is as follows

$$A(P, \beta) \simeq 1 + \frac{\alpha^2}{16\pi^2 N_f} \int_0^\alpha dK I(P, K, \beta) \frac{\tanh \left[\frac{\beta}{2} \sqrt{(K^2 + M^2(K, \beta))} \right]}{\sqrt{(K^2 + M^2(K, \beta))}}. \quad (6.23)$$

Here the mass function $M(K, \beta)$ is simply the pole mass, given by the ratio of the gap function to the wavefunction renormalization, and P, K denote spatial momentum components.

To continue it is necessary to make an *ansatz* for the kernel: replace the component Π_{00} with a constant $\Delta \sim \mathcal{O}(\alpha^2)$ [26]. With this *ansatz*

$$I = -\frac{2\pi}{P^2} \left\{ 1 - \frac{|P^2 - K^2|}{\Delta^2} + \frac{[P^2 - K^2 + \Delta^2][P^2 - K^2 - \Delta^2]}{\Delta^2 \sqrt{[(P - K)^2 + \Delta^2]} \sqrt{[(P + K)^2 + \Delta^2]}} \right\}. \quad (6.24)$$

In fact this approximation is also good for the normal phase $M = 0$. In the $P \rightarrow 0$ limit,

$$I(P = 0, K) = -\frac{4\pi(\Delta^2 - K^2)}{(\Delta^2 + K^2)^2}. \quad (6.25)$$

The effective ultra violet cut-off means that the momentum K must satisfy

$$K \in [\sqrt{(\alpha/\beta)}, \alpha].$$

Then in an intermediate momentum range

$$\sqrt{(\beta\alpha)} \sim \alpha/\varepsilon \gtrsim 1,$$

and $K \in [\sqrt{(\alpha/\beta)}, \alpha]$ to within $\mathcal{O}(\alpha)$.

Hence the wavefunction renormalization is given by

$$\begin{aligned} A(P = 0, \beta) &\simeq 1 - \frac{1}{4\pi N_f} \int_{\sqrt{(\alpha/\beta)}}^\alpha dK \frac{1}{K} \tanh \left(\frac{\beta K}{2} \right) \simeq \\ &\simeq 1 - \frac{1}{4\pi N_f} \int_{\sqrt{(\alpha\beta)/2}}^{\alpha\beta/2} dx \frac{\tanh x}{x}. \end{aligned} \quad (6.26)$$

If the temperature is very low, $\alpha\beta \gg 1$:

$$A(P = 0, \beta) \simeq 1 - \frac{1}{8\pi N_f} \ln(\alpha\beta). \quad (6.27)$$

For the region $\alpha\beta \gtrsim 1$ the integrals can be evaluated numerically and it is found that equation (6.27) is reasonably accurate:

$$\begin{aligned} \alpha\beta \gtrsim 5 &\longrightarrow \text{Result is within 10\% of (6.27);} \\ \alpha\beta \gtrsim 10 &\longrightarrow \text{Result is essentially exact.} \end{aligned} \quad (6.28)$$

The resistivity can be computed from equation (6.1) using (6.27) for the finite temperature wavefunction renormalization, with the result

$$\rho \propto T^{1-1/4\pi N_f} \quad (n = 1). \quad (6.29)$$

Note that the critical exponent is only approximate. Above it has been calculated by working in a specific gauge (the Landau gauge: $\xi = 0$) and by adopting a specific *ansatz* for the vertex, equation (4.22). However, since the resistivity is a physical gauge invariant quantity, the scaling (6.29) should be gauge-independent. This gauge-independence should be checked explicitly by either performing the computations

in many different gauges upon selecting appropriate vertex *ansätze*, or following the alternative approach to the running in theory space based on a Dyson–Schwinger treatment for the amputated vertex described in section 5.4. This method has the advantage that it avoids the problem of selecting a vertex *ansätze* satisfying the Ward–Takahashi identity, for it determines the vertex directly.

From the relation (6.28) it is apparent that this scaling is stable for a large temperature range, in agreement with the experimental situation [16, 17]. Note that the scaling exponent in relation (6.29) is *less* than one (by a small amount, at least within the $1/N_f$ treatment) in the gauge field theory model. Such a scaling seems to characterize the normal phase of the high temperature cuprates [17]. In the actual experimental observations the scaling depends on the doping concentration, δ , in such a way that the exponent diminishes linearly with δ . In the simplified field–theoretic analysis above a precise connexion between this exponent and the doping concentration cannot be made, and therefore this dependence cannot be verified directly. However, from the connexion between QED₃ and underlying statistical models [23, 48], a dependence on δ in the exponent in equation (6.29) is to be expected from the following general argument: in QED₃, $1/N_f \sim e^2/\alpha$, and from the analysis in reference [48] the coupling e^2 depends on the doping concentration. Since a detailed microscopic model is lacking at present, a phenomenological approach may be adopted to try to infer the doping dependence of the gauge coupling by comparing the resistivity curves fitted from equation (6.29) with the experimental ones [17].

6.4 Comparison with other approaches.

The scaling law (6.29) is an interesting prediction of the gauge spin–charge separation approach to high temperature superconductivity, however it may not be unique to this model. Indeed, such scaling can also be obtained in different approaches [49, 50]. In some of them [49] the non–trivial infra red fixed point structure plays a rôle in inducing the deviations from the linear resistivity in analogy with equation (6.29). In other treatments [50], a phenomenological approach to Luttinger and Fermi liquids has been adopted by combining spin–charge separation with the anomalous scaling of a Luttinger liquid in postulating the following unconventional form for the one electron retarded Green’s function [50]:

$$G_R(\vec{k}, \omega) \propto \frac{1}{\left(\omega - \epsilon_k^c + i0^+\right)^\beta \left(\omega - \epsilon_k^s + i0^+\right)^\gamma}, \quad (6.30)$$

where appropriate phase factors have been left out for simplicity. For low energy excitations near the Fermi surface

$$\epsilon_k^{c,s} = v_F^{c,s} |\vec{k} - \vec{P}_F|,$$

the indices c, s respectively denoting charge and spin degrees of freedom. In this approach spin–charge separation arises because of the different propagation velocities $v_F^{c,s}$ in a direct generalization of the one dimensional case. What the authors of [50] argue is that upon requiring time–reversal invariance (in the absence of external fields) the exponents in the Green’s function (6.30) are given by

$$\beta = \gamma = \frac{1}{2} - \chi.$$

The Fermi liquid theory corresponds to $\chi = 0$ and $v_F^c = v_F^s$, in which case the Green’s functions (6.30) have only single pole excitations corresponding to the electronic degrees of freedom. In the $\chi \neq 0$ and $v_F^c \neq v_F^s$ case there are branch cuts corresponding to spinon and holon quasiparticle excitations. The presence of the $\chi \neq 0$ exponent leads to a scaling of the direct current resistivity ρ in the normal phase of the high- T_c systems of the form

$$\rho \sim T^{1-4\chi}. \quad (6.31)$$

The authors of [50] fit this scaling with the experimental data [17] by postulating $\chi > 0$ and assuming a doping dependence. Although the method above made use of a different microscopic treatment of spin–charge separation (equation (6.14)) the similarity of the scaling laws (6.29) and (6.31) encourages further studies in order to try to establish a connexion between the two approaches.

7 Conclusions.

In these lectures a renormalization group approach to the effective field theory of condensed matter systems has been discussed. The approach proves to be extremely powerful insofar as it yields useful information on the universal behaviour of apparently different physical systems. The basic properties of the renormalization group have been described briefly, and the various effective field theory interactions have been classified according to their renormalization group scaling properties. BCS superconducting instabilities were studied by means of an exercise for the reader: they were described in terms of relevant renormalization group operators driving the theory away from the trivial infra red fixed point (Landau's Fermi liquid). Particular attention was paid to discussing quasiparticles, which are linearized excitations about the Fermi surface which exhibit appropriate scaling under the renormalization group. Such linearizations led naturally to the concept of an effective fermion "flavour number," which is the (large) number of excitations near the Landau fixed point in condensed matter systems with large Fermi surfaces. In such cases, the area of the Fermi surface may be identified (roughly) with the flavour number. Such large- N_f effective theories have a running flavour number due to the dependence in N_f on the cut-off scale in the theory.

In the second part of the lectures an interesting application of the above ideas, in particular the running flavour number, was discussed via the study of infra red structure in strongly coupled U(1) gauge theory with relativistic massless fermions. Physical arguments were given as to why such models may be relevant for the physics of high temperature superconducting cuprates.

The (non-perturbative) infra red structure of QED₃ has been studied extensively using a renormalization group improved Dyson-Schwinger approach, resummed to leading order in $1/N_f$. Self consistent solutions have been found in Landau and non-local gauges, and the importance of the infra red cut-off has been discussed. The non-trivial infra red fixed point leads to very slow running of the coupling, which may have important consequences for the physics of systems described by these models (e.g. the size of the gap and the associated coherence length in superconductors). The computation of some critical exponents using the non-local gauge and Landau-Khalatnikov transformation was also discussed.

Discontinuities arising from the removal of covariant infra red cut-offs and related Landau damping type effects in finite temperature theories have also been discussed. The connexion leads to natural predictions for the resistivity in gauge field mediated models. Gauge interactions lead to a resistivity linear in the temperature, and the slow running coupling (affecting the system through the wavefunction renormalization) alters this behaviour with $\mathcal{O}(1/N_f)$ corrections in the exponent. It is possible that these corrections are experimentally testable. In fact, recent experimental data seem consistent with slight deviations from linear T behaviour in the direct current resistivity [17].

The fundamental ideas which have been covered are as follows:

- Renormalization group analysis for U(1) gauge theories in a large- N_f framework \implies Dyson-Schwinger analysis improved by the renormalization group.
- Connexion with Landau-Fermi theory: an increase in the area of the Fermi surface corresponds to an increase in the number of flavours, and hence eventually the large- N_f limit.
- Approach the superconducting (chiral symmetry broken) phase from the normal phase.
- Use the renormalization group to investigate the evolution of Fermi surfaces in planar systems: reduction to a small momentum range in the deep infra red (in an appropriate doping regime), which admits a *relativistic* effective field theory description.
- It is found that the effective N_f (in the large- N_f regime) is renormalized, and runs with the scale: this generates a running in theory space.
- This slow running of N_f is an exclusive feature of U(1) gauge theories. The gauge interactions have a tendency to reduce the size of the Fermi surface, and hence lead to non-Fermi liquid behaviour.

Acknowledgments

N.E.M. would like to thank J. Spalek and the other organizers of the XXXVIII Cracow School of Theoretical Physics for inviting him to lecture at the School, and for providing a stimulating atmosphere during the meet-

ing. We would also like to acknowledge helpful discussions with I.J.R. Aitchison, N. Andrei, C. Hooley, M. Lavagna, J. Papavassiliou, S. Sarkar and J. Spalek. The work of N.E.M. is supported by a P.P.A.R.C. (U.K.) Advanced Research Fellowship. A.C.-S. would like to thank P.P.A.R.C. (U.K.) for a research studentship (number 96314661).

References

- [1] K. Wilson, *Reviews of Modern Physics* **47**, 773 (1975).
- [2] J. Polchinski, TASI Lectures (1992): *hep-th/9210046*.
- [3] R. Shankar, *Physica A* **177**, 530 (1991).
- [4] G. Benfatto and G. Gallavotti, *Physical Review B* **42**, 9967 (1990).
- [5] L. Kadanoff, in *Proceedings of the “Enrico Fermi” International School of Physics*, edited by M. Green (Academic Press, New York, 1971).
- [6] K. Wilson and M. Fisher, *Physical Review Letters* **28**, 240 (1972).
- [7] K. Wilson and J. Kogut, *Physics Reports* **12**, 75 (1974).
- [8] I.J.R. Aitchison and N.E. Mavromatos, *Physical Review B* **53**, 9321 (1996).
- [9] A. Zamolodchikov, *JETP Letters* **43**, 730 (1986), *Soviet Journal of Nuclear Physics* **46**, 1090 (1987).
- [10] N.E. Mavromatos, J. Miramontes, and J. de Santos, *Physical Review D* **40**, 535 (1989).
- [11] For a recent attempt, see S. Forte and J. Latorre, *hep-th/9805015* and references therein.
- [12] A. Ludwig and J. Cardy, *Nuclear Physics B* **285**, 687 (1987).
- [13] J. Kondo, *Progress of Theoretical Physics* **32**, 37 (1964).
- [14] J. Luttinger and J. Ward, *Physical Review* **118**, 1417 (1960).
- [15] R. Shankar, *Reviews of Modern Physics* **66**, 129 (1994).
- [16] C. Varma *et al.*, *Physical Review Letters* **63**, 1996 (1989), and references therein.
- [17] A. Malinowski *et al.*, *Physical Review Letters* **79**, 495 (1997).
- [18] J. Polchinski, *Nuclear Physics B* **422**, 617 (1994).
- [19] I.J.R. Aitchison, G. Amelino-Camelia, M. Klein-Kreisler, N.E. Mavromatos and D. McNeill, *Physical Review B* **56**, 2836 (1997).
- [20] I.J.R. Aitchison, N.E. Mavromatos, and D. McNeill, *Physics Letters B* **402**, 154 (1997).
- [21] K. Kondo, *Physical Review D* **55**, 7826 (1997).
- [22] C. Tsuei *et al.*, *Physical Review Letters* **73**, 593 (1994); K. Moler *et al.*, *ibid.* **73**, 2744 (1994); D.A. Bonn *et al.*, *ibid* **68** 2390, (1992).
- [23] N. Dorey and N.E. Mavromatos, *Physics Letters B* **250**, 107 (1990); N. Dorey and N.E. Mavromatos, *Nuclear Physics B* **386**, 614 (1992). For a comprehensive review, see N.E. Mavromatos, *Nuclear Physics B Proceedings Supplements C* **33**, 145 (1993).
- [24] L. D. Debbio and S. Hands, *Nuclear Physics B* **502**, 269 (1997).
- [25] K. Kondo and H. Nakatani, *Progress of Theoretical Physics* **87**, 193 (1992).

- [26] I.J.R. Aitchison and M. Klein-Kreisler, *Physical Review* **D 50**, 1068 (1994).
- [27] K. Kondo and H. Nakatani, *Modern Physics Letters* **A 4**, 2155 (1989).
- [28] T. Appelquist, M. Bowick, D. Karabali, and L. Wijewardhana, *Physical Review* **D 33**, 3704 (1986).
- [29] M. Pennington and S. Webb, BNL preprint-40886 (January 1988) (unpublished).
- [30] D. Atkinson, P. Johnson, and M. Pennington, BNL preprint-41615 (August 1988) (unpublished).
- [31] K. Higashijima, *Physical Review* **D 29**, 1228 (1984).
- [32] P. Maris, *Physical Review* **D 54**, 4049 (1996).
- [33] I.J.R. Aitchison and J. Zuk, *Annals of Physics* **242**, 77 (1995).
- [34] A. Campbell-Smith, *Modern Physics Letters* **A 13**, 2337 (1998).
- [35] J. Cornwall, R. Jackiw, and E. Tomboulis, *Physical Review* **D 10**, 2428 (1974).
- [36] G. Amelino-Camelia, *Physical Review* **D 49**, 2740 (1994).
- [37] T. Appelquist, J. Terning, and L. Wijewardhana, *Physical Review Letters* **79**, 2767 (1997).
- [38] L. Landau and I. Khalatnikov, *Soviet Physics JETP* **2**, 69 (1956).
- [39] I.J.R. Aitchison, *Zeitschrift für Physik* **C 67**, 303 (1995).
- [40] D. Nash, *Physical Review Letters* **62**, 3024 (1989).
- [41] K. Kondo and T. Murakami, *Physics Letters* **B 410**, 257 (1997).
- [42] N.E. Mavromatos and J. Papavassiliou, work in progress.
- [43] J. Papavassiliou and J. Cornwall, *Physical Review* **D 44**, 1285 (1991).
- [44] P. Anderson, *Science* **235**, 1196 (1987).
- [45] L. Ioffe and A. Larkin, *Physical Review* **B 39**, 8988 (1989).
- [46] N. Nagaosa and P. Lee, *Physical Review Letters* **64**, 2450 (1990); L. Ioffe and P. Wiegmann, *ibid.* **65**, 653 (1990).
- [47] J. Latorre, P. Pascual, and R. Tarrach, *Nuclear Physics* **B 437**, 60 (1995).
- [48] N. Dorey and N.E. Mavromatos, *Physical Review* **B 44**, 5286 (1991).
- [49] C. Nayak and F. Wilczek, *Nuclear Physics* **B 417**, 359 (1994), and cond-mat/9507040 (*International Journal of Modern Physics* **B** (1995)).
- [50] K. Byczuk *et al.*, *Luttinger-liquid phenomenology for high- T_c superconductors*; K. Byczuk, J. Spałek and W. Wójcik, *Luttinger-liquid phenomenology: applications to high temperature superconductors*; Warsaw and Cracow Jagiellonian University preprints (1998).